Title

CHARGE-EXCHANGE PRODUCTION OF ANTI-NEUTRONS AND THEIR ANNIHILATION IN HYDROGEN

Authors

Hinrichs, C.K.
Moyer, B.J.
Poirer, J.A.
et al.

Publication Date

1961-07-05

UCRL-9589 Rev.

UNIVERSITY OF CALIFORNIA

Ernest O. Lawrence Radiation Laboratory

BERKELEY, CALIFORNIA

DISCLAIMER

UCRL-9589 Rev.

UNIVERSITY OF CALIFORNIA
Lawrence Radiation Laboratory
Berkeley, California

Contract No. W-7405-eng-48

CHARGE-EXCHANGE PRODUCTION OF ANTINEUTRONS AND THEIR ANNIHILATION IN HYDROGEN

C. Keith Hinrichs, Burton J. Moyer, John A. Poirer, and Philip M. Ogden

July 5, 1961

CHARGE-EXCHANGE PRODUCTION OF ANTINEUTRONS AND THEIR ANNIHILATION IN HYDROGEN

C. Keith Hinrichs, Burton J. Moyer, John A. Poirier, and Philip M. Ogden

Lawrence Radiation Laboratory
University of California
Berkeley, California

July 5, 1961

ABSTRACT

The charge exchange of antiprotons into antineutrons and the subsequent annihilation of antineutrons have been studied in the 72-inch liquid hydrogen bubble chamber. The antiprotons were produced internally in the Bevatron; channeled externally by collimation, quadrupole fucusing magnets, and bending magnets; and separated from other negatively charged particles by a system of three velocity spectrometers. Analysis of the data for a run with an antiproton momentum of 1.65 Bev/c has been completed. Three charge-exchange reactions have been studied: (1) $\bar{p} + p \rightarrow \bar{n} + n$, (2) $\bar{p} + p \rightarrow \bar{n} + n + \pi^0$, (3) $\bar{p} + p \rightarrow \bar{n} + p + \pi^-$. The cross section for Reaction (1) plus Reaction (2) was $7.82 \pm .55$ mb. The cross sections for Reaction (3) was $0.99 \pm .24$ mb, which implies on the basis of the statistical model alone that the cross section for Reaction (2) is also about 1 mb. The angular differential cross section for Reaction (1) was strongly peaked forward with a value at zero degrees of $4.6 \pm .5$ mb/sr. However, the 13% contamination from (2) was included. Of the antineutrons produced in Reactions (1) and (2), 122 annihilated in the bubble chamber; the resulting annihilation cross section was 45.2 ± 5.4 mb at a lab kinetic energy of 900 Mev. The average charged-pion multiplicity in the antineutron annihilations was found to be $3.5 \pm .3$, which implied that the total pion multiplicity was $5.2 \pm .4$. The ratio of the number of antineutron annihilations containing five charged pions to the number containing three charged pions, and

the momentum distribution of the pions, have been compared with predictions of the statistical model. This model used the covariant phase-space integrals first proposed by Srivastava and Sudarshan and modified by Neuman, and the branching ratios given by Pais. Reasonable agreement was obtained for a volume five times that of a sphere with a radius of one pion Compton wave length. The center-of-mass angular distribution of the pions in the antineutron annihilations was found to be, within statistics, and isotropic distribution. Three events were found that fitted K^0-meson production in antineutron annihilation.

CHARGE-EXCHANGE PRODUCTION OF ANTINEUTRONS* AND THEIR ANNIHILATION IN HYDROGEN*

C. Keith Hinrichs†, Burton J. Moyer, John A. Poirer, and Philip M. Ogden

Lawrence Radiation Laboratory
University of California
Berkeley, California

July 5, 1961

I. INTRODUCTION

After several unsuccessful attempts, the antineutron was identified by a counter experiment in 1956.[1] The antineutrons were produced by the charge exchange of antiprotons on protons ($\bar{p} + p \rightarrow \bar{n} + n$) and identified by the large annihilation energy of the antineutrons in a counter. Other counter experiments have studied the charge-exchange reaction on hydrogen[2-4] as well as on complex nuclei,[5] and in 1959 the charge exchange of an antiproton into an antineutron and the subsequent annihilation of the antineutron were first observed in a propane bubble chamber.[6] In all these experiments it was assumed that the annihilation cross section for antineutrons was the same as that for antiprotons, in order to estimate the charge-exchange cross sections. In these previous experiments, the small value of the charge-exchange cross section, combined with the rarity of antiprotons themselves, permitted little more than confirmation of the process, and little light could be shed on the antineutron interactions, including antineutron annihilation.

The antineutron interactions in hydrogen are of particular interest because the reaction occurs in a pure isotopic spin triplet state ($T = 1$), whereas the antiproton-proton interaction is composed of half isotopic singlet ($T = 0$) and half isotopic triplet states. It is to be noted that antiproton-neutron interactions also occur in the pure isotopic triplet state, and in this respect should be the same as $\bar{n}$-p interactions. Some recent results on antiproton-neutron interactions have been obtained by deuterium-hydrogen subtraction.[7]

The experiment presented here sends a separated beam of 950-Mev antiprotons into the 72-inch hydrogen bubble chamber, and studies not only the charge-exchange interactions and their angular distribution but also the nature of the antineutron-proton annihilation.

The performance of this experiment was ancillary to an experiment that successfully searched for the antilambda in the reaction $p + p \rightarrow \bar{\Lambda} + \Lambda$.[8,9] This reaction has a threshold at antiproton energies of about 770 Mev, and dictated the energy of antiprotons used.

II. DESCRIPTION OF THE EXPERIMENT

A. The Antiproton Beam

Antiprotons produced internally in the Bevatron were extracted and sent through a separating system to purify the antiproton beam. This system was patterned after the 1.17-Bev/c K^- beam of Eberhard, Good, and Ticho.[10, 11] The beam design consisted of quadrupole focusing magnets, Q, velocity-selecting spectrometers, SP, iron collimating slits, S, and bending magnets, BM, arranged as shown in Fig. 1. The purified beam of antiprotons was then directed into the 72-inch hydrogen bubble chamber where the various interactions were photographed. The circulating Bevatron beam of 6.2-Bev protons struck the aluminum target, producing the antiprotons. Those antiprotons with momentum 1.64 Bev/c passed through a hole in an iron nose cone (labeled NC on Fig. 1) in the outer magnetic yoke of the Bevatron magnet, and entered the separator system.

The ratio of π^- mesons to antiprotons produced was of the order of a few times 10^4, and the elaborate beam optics of the experiment was required to separate the antiprotons from this overwhelming number of unwanted particles. Since a Detailed descritpion of the beam design has been given previously,[9] only the characteristics of the target, the beam, and the optical system are presented here in Table I. A monitor telescope (labeled MT on Fig. 1) was set up to look at 1-Bev/c π^- mesons coming from the target, and by this means to indicate the relative number of protons striking the target.

B. The 72-Inch Liquid Hydrogen Bubble Chamber

The bubble chamber is roughly 72 in. long by 20 in. wide by 15 in. deep.[12] The 1-msec beam spill occurred at the center of the sensitive time of the bubble chamber (approximately 15 msec, under the operating conditions of this experiment). The light flash for the pictures occurred about 4 msec after the beam spill, which

allowed sufficient time for bubble growth and kept distortion due to turbulence insignificant. The rate of energy loss by ionization for antiprotons and pions in the beam differed by only about 2%, therefore no attempt was made to differentiate antiproton tracks from pion tracks on the basis of bubble counting. The average density of the hydrogen during beam spill has been measured as 0.0586 g/cm^3.

The bubble chamber magnet supplied an average field of 17.9 kgauss, with a measured variation over the volume of the chamber of approximately ± 10%

After each expansion three cameras located at three corners of a square took stereoscopic pictures of the chamber (this square was 20 in. on a side, located 74 in. above the chamber).

The magnetic-field corrections and optical corrections for each of the three views as a function of position in the bubble chamber were taken into account in the analysis of the track photographs.

III. ANALYSIS OF DATA

A. Classification of Reaction Types

The beam entering the bubble chamber was composed primarily of μ^- and π^- mesons and antiprotons. The μ^- mesons did not interact in the chamber and contributed only to the number of background tracks. The π^- mesons could interact strongly, however, and constituted the largest source of corrections to the number of antiproton interactions.

The reactions with which this experiment was primarily concerned are

$$\bar{p} + p \rightarrow \bar{n} + n, \qquad \text{elastic charge exchange;} \tag{1}$$

$$\left.\begin{aligned} \bar{p} + p &\rightarrow \bar{n} + n + \pi^0 \\ \bar{p} + p &\rightarrow \bar{n} + p + \pi^- \end{aligned}\right\} \qquad \text{inelastic charge exchange;} \tag{2, 3}$$

$$\bar{n} + p \rightarrow \pi\text{'s and K's} \qquad \text{antineutron annihilation.} \tag{4}$$

The inelastic charge-exchange reactions producing more than one pion were presumed to be unimportant and were neglected. (It will be shown in the next section that inelastic charge exchange with one pion produced is only about 13% of Reaction (1), therefore it was assumed that the charge exchange with two-pion production is even smaller. In fact no events were found to fit the reaction $\bar{p} + p \rightarrow \bar{n} + n + \pi^+ + \pi^-$).

The antiprotons also annihilated in various ways, some of which could be confused with the charge-exchange reactions

$$\bar{p} + p \rightarrow (\ell + 2)\pi^0, \tag{5}$$

$$\bar{p} + p \rightarrow \pi^+ + \pi^- + \ell\,\pi^0, \tag{6}$$

$$\bar{p} + p \rightarrow 2\pi^+ + 2\pi^- + \ell\pi^0, \tag{7}$$

$$\bar{p} + p \rightarrow \pi\text{'s and K's}, \tag{8}$$

where $\ell = 0, 1, \ldots$; ℓ is limited by the energy available in the reaction.

The pions could interact as follows:

$$\pi^- + p \rightarrow \pi^0 + n + \ell\pi^0, \tag{9}$$

$$\left.\begin{aligned} \pi^- + p &\rightarrow \pi^- + p + \ell\pi^0 \\ &\rightarrow \pi^+ + \pi^- + n + \ell\pi^0 \end{aligned}\right\} \tag{10}$$

$$\pi^- + p \rightarrow 2\pi^- + p + \pi^+ + \ell\pi^0, \text{ etc.} \tag{11}$$

Reactions (1), (2), (5), and (9) could not be differentiated in the bubble chamber and were characterized by a beam track entering the chamber and ending in the volume of hydrogen. This type of event was designated as a 0-prong. Reactions (3), (6), and (10) could not be differentiated by inspection if the proton in Reactions (3) and (10) did not stop in the chamber, and were all designated as 2-prong interactions. Similarly, Reactions (7) and (11) were designated as 4-prong interactions. A few antiprotons were observed to annihilate into six and eight charged pions, and were designated 6-prong and 8-prong, respectively.

The annihilation of an antineutron (Reaction 4) produced a "neutral star" (i.e., a star produced by a neutral particle) with one more positive track than the number of negative tracks. Thus $\bar{n}$ annihilations were designated as 1-, 3-, 5-, or 7-prong.

Figure 2 is a bubble chamber photograph of a 5-prong $\bar{n}$ annihilation. The antineutron is presumed to have been produced at the 0-prong ending.

A 2-prong event fitting Reaction (3) is shown in Fig. 3. Here the antineutron annihilated into a 3-prong star.

B. Scanning and Measuring of Events

Approximately 46,000 bubble chamber pictures were taken. (Each picture consisted of three stereoscopic views.) They were all scanned by using scanning tables especially constructed to view the 72-inch bubble chamber film. A "useful volume" was defined for the bubble chamber, which excluded

areas where the film showed poor track visibility or where the proximity of a physical boundary reduced the probability of observing an interaction. Interactions occurring outside this volume were disregarded.

For a track to be considered a beam track, it was required to satisfy three criteria on the scanning table; it must:

1. enter the chamber at an angle within 5 degrees of the average direction of the beam tracks,

2. have a curvature corresponding to a momentum of 1.6±.2 Bev/c (see Fig. 4),

3. cross the entrance boundary to the "useful volume."

According to the scan criteria, a neutral star was any interaction that did not:

1. contain an incident beam track,

2. have a positively charged stopping track (i.e., have an identifiable proton emerging),

3. have one positive and one negative track (a "V").

Because a large number of recoil protons occurred in the chamber, interactions consisting of one positive track leaving the chamber were not considered as neutral stars.

Scanning efficiencies for each type of event were determined by making two separate scans of the same film.

Measurement of angles and momenta on the scanning table were difficult and inaccurate. To facilitate measurement of events, use was made of the Franckenstein measuring projector,[13] which determined a succession of track coordinates in two of the three stereoscopic views. An IBM 704 computer program called PANG ("P" for momentum and "ANG" from angle)[14] was used to analyze the track coordinates and calculate the track reconstruction. Momentum,

position, azimuthal angle, and dip angle at the beginning and end of the track were calculated.

C. Determination of Beam Composition

The total number of tracks, corrected for a scanning efficiency of 95%, was 191,000. These tracks were due to antiprotons, pions, muons, and K particles. The muons did not interact, and the number of K particles was negligible. (The number of K particles, 100, was determined from 10 K decays in flight.[9]) It was possible, therefore, to obtain the number of pion and $\bar{p}$ tracks from the number of pion and $\bar{p}$ interactions and their known total interaction cross sections.

The number of pion interactions was determined from the number of δ rays with kinetic energy greater than 6.0 Mev occurring on interacting tracks. (It is energetically impossible for a 1.63-Bev/c antiproton to produce a δ ray with energy greater than 3.1 Mev.[15]) A little more than one-third of the film was scanned for such δ rays. Using the known cross section for production of δ rays with energy greater than 6.0 Mev by 1.5-Bev/c pions[16]--that is, 32 mb[17]--we determined the number of pion interactions. This number, when corrected for scanning efficiency, was $(3.2 \pm 0.4) \times 10^3$. The remaining 18,700 interactions were attributed to antiprotons.

The total $\bar{p}$ cross section, 98 ± 3 mb,[3,4] was reduced by 8% to account for scattering of less than 4.5 deg, which could not be detected reliably. From this reduced cross section and the effective path length in the useful volume of the bubble chamber, 62 in., we obtained a probability of 0.40 for production of observable antiproton interactions. From these numbers we concluded that 46,800 antiprotons entered the useful volume of the bubble chamber. Similarly, taking the pion cross section of 34.5 ± 1.0 mb,[18] and making a 2.6% correction

for small-angle scattering, we found that 18,900 pions entered the useful volume of the bubble chamber.

The relative beam composition given in Table I was obtained from the above numbers. There were 43,100 "good" frames, which gave an average of 1.1 $\bar{p}$ per frame, with 4.4 tracks per frame.

D. Method Used to Calculate the $\bar{n}$ Annihilation Cross Section

To determine the annihilation cross section for antineutrons we must know the total number of antineutrons produced by the 0-prong process (Reactions 1 and 2) and the events in which an $\bar{n}$ star was associated with a 0-prong. The number of $\bar{n}$'s produced in the 2-prong interaction was relatively small and was difficult to determine. Therefore only the 0-prong production of antineutrons was considered in determining the annihilation cross section

1 Determination of the number of antineutrons produced by the 0-prong process

The actual value of $N_0^{\bar{n}}$ will now be determined. The number of 0-prongs that gave antineutrons was given by

$$N_0^{\bar{n}} = N_0 - N_{0\pi} - N_{0\bar{p}\,\mathrm{ann.}} - N_0^{v}, \qquad (12)$$

where N_0 = number of 0 prongs occurring,

$N_{0\pi}$ = number of 0-prongs produced by pions,

$N_{0\bar{p}\,\mathrm{ann.}}$ = number of 0-prong annihilations,

N_0^{v} = number of antiprotons that produced $\Lambda\bar{\Lambda}$ pairs

The value of N_0 was determined to be 2149 from film scans corrected for a combined scanning efficiency of 0.98.

The number N_0^{v} has been determined to be 11, by independent work.[9]

The number $N_{0\pi}$ was obtained from the total number of pion interactions, $(3.2 \pm .4) \times 10^3$, and from the ratio of the cross section for 0 prong production by

pions, 4 75 ± .25 mb,[19] to the total pion interaction cross section corrected for small-angle scattering. The value for this number was $N_{0\pi} = 453 \pm 61$. This will turn out to be the largest subtraction in Eq. (12). Therefore the method used to determine $N_0^{\bar{n}}$ is quite valid.

An estimate for $N_{0\bar{p}\ ann}$ was obtained from a scan for electron-positron pairs pointing at the end of a 0-prong beam track. These pairs were produced by decay γ rays coming from the π^0's produced by the 0-prong It was found that 946 ± 195 π^0's were produced by 0-prongs.

The 0-prong reactions (2), (5), and (9) all give π_0 mesons.

The average number of π^0's produced by Reaction (9) is about $1.1 \pm .1$.[20] Then the number of π^0's produced by 0-prong pion events is $1.1\ (N_{0\pi}) = 498 \pm 81$.

The cross section for Reaction (2) can be estimated from the cross sections for Reaction (3) and the reaction $p + \bar{p} \rightarrow n + \bar{p} + \pi^+$. Both of these turn out to be about 1 millibarn.[21] Then on the basis of the statistical model alone, the cross section for Reaction (2) should be about 1 mb.

If the cross sections for Reactions (2) and (3) are assumed to be the same, the same number of events for each should occur.[22] The number for Reaction (3) is calculated in Section IV-C as 205 ± 50. Subtracting the numbers of π^0's from Reactions (9) and (2) from the total number of π^0's coming from 0-prongs, we obtain 243 ± 217 π^0's due to 0-prong annihilation. The statistical model (see Appendix) predicts that the average pion multiplicity in 0-prong annihilations is 4. Then the number of 0-prong annihilations, $N_{0\bar{p}\ ann}$, is 61 ± 54.

When these numbers (with their associated errors) are combined in Eq. (12), the actual number of antineutrons produced in 0-pronge is

$$N_0^{\bar{n}} = 2149 - 453 - 61 - 11 = 1624 \pm 94.$$

2. Identification of the annihilation stars associated with a 0-prong.

For a neutral star to be associated with a 0-prong it was first required that the star occur in the forward hemisphere with respect to the 0-prong. (It was kinematically impossible in the laboratory frame of reference for an antineutron to have a momentum component backward with respect to the antiproton.) The star was then analyzed to determine that it actually was an antineutron star. To do this, the 0-prong and associated star were measured and processed by PANG. The output from PANG was coded for an IBM 650 program called ANSAN (AntiNeutron Star ANalysis), which performed the relativistic kinematic calculations. Assuming Reaction (1) for the antineutron production, we determined the laboratory-frame antineutron energy and the center-of-mass angle between the $\bar{n}$ and $\bar{p}$ directions. In addition, the energy of the pions in the star and their momentum components parallel and perpendicular to the antineutron direction were calculated. For three-prong stars a coplanarity factor, which indicated whether the three tracks were coplanar, was also calculated. Events that were coplanar were analyzed for momentum balance to determine if the star was actually a scattering event, and thus not an antineutron annihilation.

The ANSAN output was analyzed to determine that (a) the energy of the star was too great for it to be due to other than annihilation, and (b) the visible energy and momentum unbalance, if any, were compatible with an $\bar{n}$ annihilation, with the $\bar{n}$ coming from the 0-prong.

A scan was made to obtain the number of stars occurring in the backward hemisphere of the 0-prong. This gave an estimate of the number of events that were incorrectly assumed to be associated. These were called false associations. There were several cases in which more than one 0-prong occurred on the same frame with a possible $\bar{n}$-star association. This gave an independent determination of the number of false associations.

The numbers of real and false associations are given in Section IV.

3. The determination of the antineutron annihilation cross section

For each associated star-0-prong event, i, with lab angle θ_i between the $\bar{n}$ and $\bar{p}$ directions, the probability P_i of visible occurrence of the event was calculated. The weight $W_i = 1/P_i$ for each event could be thought of as the number of antineutrons that must have been produced at angle θ_i so that the event was seen. The total number of antineutrons produced by 0-prongs that would annihilate into more than one charged pion would then be given by the sum of the weights for all associated events, $\sum_i W_i$. This had to be corrected to account for 1-prong annihilations in order to obtain the total number of antineutrons, as is discussed later.

The probability of seeing an annihilation was given by the formula $p = 1 - \exp(-\ell n \sigma_a')$, where ℓ is the distance the $\bar{n}$ could have gone before leaving the useful bubble chamber volume, σ_a' is the cross section for antineutron annihilation into more than one prong, and n is the density of protons in the liquid hydrogen.

Smaller statistical errors are obtained if the probability p is averaged over position and azimuthal angle. This was done by WEIGHT, and IBM 704 program. Given the position, direction, and momentum of the $\bar{p}$ track at its beginning, this program reconstructed the $\bar{p}$ path through the chamber. At each of six equally spaced points along this projected path and for the given angle θ_i, ℓ was determined for each of eight equally spaced azimuthal angles about the $\bar{p}$ direction. Then p was determined for each ℓ and an average was taken. Each of the six points was weighted to account for the attenuation of the antiproton beam in passing through the chamber. In this way WEIGHT calculated P_i (equal to the averaged p) and W_i for each event.

This antineutron energy (a function of the angle θ_i) varied over a large range (Fig. 5). To allow an energy dependence for the annihilation cross section,

the formula

$$\sigma_a = \pi(a + \lambda)^2 \qquad (13)$$

was used, where λ is the center-of-mass de Broglie wavelength for the antineutron and a is a core radius. This formula was first proposed in connection with nucleon antinucleon annihilation, by Koba and Takeda.[23]

Since it was not possible to scan for 1-prong annihilations, the W_i calculated gave only the number of antineutrons that would have annihilated into more than one charged pion. To correct for this, each W_i was multiplied by a factor K_i, which was a function of the energy of the $\bar{n}$ in that event. This factor was calculated from predictions of the statistical model for annihilation and the branching ratios for the various modes of annihilation (see Eq. (A-7) of the Appendix). Then $\sum_i K_i W_i$ was the total number of antineutrons produced by 0-prongs. This number was finally corrected for scanning efficiency and false associations:

$$N_0^{\bar{n}} = \frac{1}{\text{Efficiency}} \left(\frac{\text{Total - False}}{\text{Total}} \right) \sum_i K_i W_i \, . \qquad (14)$$

This predicted value of $N_0^{\bar{n}}$ was determined for several values of a. With the actual value of $N_0^{\bar{n}}$ determined above from the number of 0-prongs observed, the proper choice of a can be made, and σ_a can then be calculated from Eq. (13).

IV. EXPERIMENTAL RESULTS

A. Number and Classification of Associated Antineutron Stars

Summaries of the associated stars and their classifications will be found in Tables II and III.

Eighty-seven possible associations of 0-prongs with 3-prong stars (designated (0, 3) events) were found. Of these, 83 occurred in the useful bubble chamber volume. The 3-prong stars of six events fitted π-p or p-p scattering; that is, the three tracks were coplanar and the momentum balanced. (These events occurred for unassociated π's or p's that were not beam tracks.) All the remaining 77 events were assumed to be good events. Two of the events could not be measured or analyzed accurately because of a missing stereo view or obstruction of the event by bubble chamber hardware in one view. These two events appeared to be good in all respects, and since only six events were rejected out of 83, it was thought best to include them. Seventy-five (0, 3) events were measured, and all except one were found to be compatible with antineutron annihilation, with the $\bar{n}$ produced at the 0-prong. The one event that did not fit had too much visible energy in the star to have been produced by an $\bar{n}$ associated with the 0-prong. The star tracks were not coplanar, however, and one track had a large error in momentum; therefore the event was assumed to be good.

Fifty-one possible associations of 0-prongs with 5-prong stars, (0, 5) events, were found, Forty-four occurred in the useful volume. All the measurable events were compatible with antineutron annihilation, with the $\bar{n}$ produced at the 0-prong; however, six of the 44 events were unmeasurable. All six unmeasurable events appeared to be good in all respects and were included.

Only one association of a 0-prong with a 7-prong star was found, and it was compatible with $\bar{n}$ production at the 0-prong.

The "good events" were classified as to the reliability of their being the desired interactions. This was done as follows. The measurable events were analyzed by the ANSAN program described in Sec. III-D-2). It was assumed that the star was not an annihilation but a nucleon-nucleon or π-nucleon interaction, with two of the positive tracks due to protons, and the minimum visible energy U_{min}^{vis} was calculated. U_{min}^{vis} included the kinetic energy of the two particles assumed to be protons and the total energy of the other particles, which were assumed to be pions. The maximum kinetic energy of a nucleon or a pion was presumed to be less than 1 Bev (the kinetic energy of the antiprotons entering the bubble chamber was about 950 Mev). Thus if U_{min}^{vis} was found to be greater than 1 Bev, the event could not have been due to other than annihilation and was given the reliability classification I. If U_{min}^{vis} was greater than the kinetic energy of a neutron coming from the 0-prong, but less than 1 Bev, the event was given classification II. Finally, if U_{min}^{vis} plus the energy required to balance momentum (assuming the neutron was produced at the associated 0-prong) was determined to be greater than 1 Bev, the event was given classification III. Unmeasurable events are listed under classification IV. See Table II.

The number of false associations was estimated in three ways:

1. Of the above events, two(0, 3) events and two (0, 5) events had two 0-prongs on the same frame, and one (0, 5) event had three 0-prongs on the same frame. Thus, if each 0-prong star were counted as an association, there would be at least 6 false associations in 128 events. If we assume this ratio to hold, then there were $(6/128)\times 122 = 5.7$ false associations in the 122 events in Table II.

2. A scan was made for 5- or 7-prong stars occurring behind a 0-prong. Two such events were found. Since there are 77/45 times as many 3-prongs as 5- and 7-prongs, $2 + (77/45)\times 2 = 5.4$ $\bar{n}$ stars are expected to occur behind 0-prongs. The average length of a 0-prong track is about one-half the bubble

chamber length, and if the nonassociated $\bar{n}$ stars are uniformly distributed throughout the chamber (which is a suitable approximation here), then equal numbers of nonassociated stars should occur before and after the 0-prong ending. This implies that about 5.4 false associations occur in the 122 events as listed in Table II.

3. There were found about 220 nonassociated antineutron stars and about 2149 - 122 = 2027 nonassociated 0-prongs (where 2149 is the total number of 0-prongs and 122 is the number of associated events). These occurred on about 43,000 pictures. Then the number of cases having an unassociated 0-prong and star on the same frame is

$$\frac{2027}{43,000} \times \frac{220}{43,000} \times 43,000 = 10.2$$

If the stars are uniformly distributed and the average 0-prong length is one-half the bubble chamber length, half of these cases will occur before the 0-prong ending and half will occur after. Thus, again we arrive at about 5.1 false associations.

B. The Annihilation Cross Section

We calculated the ratio of 5-prong to 3-prong stars, using those events which had an antineutron laboratory-frame kinetic energy between 800 Mev and 1000 Mev. In this range there were 33 5-prongs and 63 3-prongs, which gave a ratio $R = 0.52 \pm .11$. The average kinetic energy for the 96 events was 894 Mev. This ratio is plotted in Fig. 6 along with predictions of the statistical model, as a function of $\bar{n}$ kinetic energy, for various values of the volume parameter, λ (see Appendix). A fit is obtained for $\lambda = 5 \pm 1$.

With the choice of $\lambda = 5$, the correction factor for 4-prong annihilation, K, was calculated as a function of antineutron laboratory-frame kinetic energy,

and is plotted in Fig. 7. Since the antineutron energy is determined an appropriate value for K could be chosen for each event.

The combined scanning efficiency for seeing 0-prong–star associations for 3-, 5-, and 7-prong stars was 0.975, and the number of false associations was taken to be 5.5. Putting these numbers into Eq. (14), with a correction to account for the fact that only 117 of the 122 events were measured and weighted, gave us

$$N_0^{\bar{n}} = 1.021 \sum_{i=1}^{117} W_i K_i. \qquad (15)$$

The summation $\sum W_i K_i$ was determined for five values of the core radius, a that is, a = 0.80, 0.85, 0.90, 0.95, 1.00 fermi (1 fermi = 10^{-13} cm). The resulting values for $N_0^{\bar{n}}$ and their errors are plotted in Fig. 8. The errors were determined from

$$\left[\sum_i (W_i K_i)^2\right]^{1/2}.$$

The actual value for $N_0^{\bar{n}}$ obtained in Section III-D-1 is also plotted as a line at $N_0^{\bar{n}} = 1624$, with errors ±94. The intersection of the two curves occurs at a = 0.896.

The values of the $N_0^{\bar{n}}$ obtained from both determinations are assumed to follow the Gaussian, or normal, error law. The ellipse in Fig. 8 is then the locus of points where the product of the probability amplitudes for the two distributions corresponds to the value at one standard deviaiton. The error in a is taken to be the maximum excursion of this ellipse parallel to the a axis. Thus, $a = 0.896 \pm .072$, and from Eq. (13) the annihilation cross section at 900 Mev is

$$\sigma_a(\bar{n}\text{-}p) = 45.2 \pm 5.4 \text{ millibarns}.$$

C. The Charge-Exchange Cross Sections

The total charge-exchange cross section by the 0-prong mode is obtained from the equation

$$\sigma_{ce}(0\text{-prong}) = \frac{N_0^{\bar{n}}}{\text{total number of observable } \bar{p} \text{ interactions}} \sigma_t'(\bar{p}p), \qquad (16)$$

where $\sigma_t'(\bar{p}p)$ is the total $\bar{p}$-p cross section corrected for small-angle scattering. An 8% correction to the total cross section for unobservable small-angle scattering gives

$$\sigma_t'(\bar{p}\text{-}p) = 90.2 \pm 3 \text{ mb}.$$

Then

$$\sigma_{ce}(0\text{-prong}) = 7.82 \pm .55 \text{ mb}.$$

The differential cross section as a function of angle was obtained by summing the corrected weights for events in each interval $\Delta(\cos\theta_j)$ and normalizing this sum to the total cross section,

$$\frac{d\sigma_{ce}}{d\Omega}(\cos\theta_j) = \frac{\left(\sum_k W_{kj} K_{kj}\right)\cos\theta_j}{\sum_j \left(\sum_k W_{kj} K_{kj}\right)\cos\theta_j} \cdot \frac{\sigma_{ce}\,(0\text{-prong})}{2\pi\,\Delta(\cos\theta_j)}, \qquad (17)$$

where θ is the center-of-mass angle between the $\bar{n}$ and $\bar{p}$ directions. This distribution is plotted in Fig. 9 together with the angular distribution of the 117 events. The value at zero degrees is

$$\frac{d\sigma_{ce}\,(0\text{ deg})}{d\Omega} = 4.6 \pm .5 \text{ mb/sr}.$$

To determine the cross section for inelastic charge exchange by Reaction (3), $\bar{p} + p \rightarrow \bar{n} + p + \pi^-$, each possible star–2-prong association was measured and processed by PANG. The star was analyzed as described above to determine if it was an antineutron annihilation. With only the energy of the $\bar{n}$ to be solved for in the above reaction, the problem is overdetermined. Two methods were used to fit the events. The ANSAN program calculated the $\bar{n}$ direction from the kinematics of the 2-prong interaction. A plot of the difference between the calculated direction and the measured direction obtained from the purported $\bar{n}$ annihilation point for each event indicated those events which fitted the reaction. Another program, KICK[24] was also utilized to fit the interaction. This IBM 704 program adjusted the measured quantities of the 2-prong and the $\bar{n}$ direction under the constraints of energy and momentum conservation to give the best fit as determined by the smallest χ^2 value.

Seventy possible 2-prong–star associations were processed by KICK. This included 17 out of 20 events classified as "good" by the ANSAN analysis. Remeasurement was required for the other three events in order to be processed by KICK, but

was not possible because of damage to the film. The plot of χ^2 for the 70 events is given in Fig. 10. Of the twenty events found to fit Reaction (3) for antineutron production with an associated antineutron annihilation star, one occurred outside the useful bubble chamber volume and could not be included in the cross-section calculation. Another event occurred for an antiproton that had already scattered elastically. Since it had already interacted, it also could not be included in the cross-section calculation. The laboratory-frame kinetic energy of the antineutrons produced in the 2-prong interaction is plotted in Fig. 11 for the 19 events occurring on unscattered $\bar{p}$ tracks.

The sum of the weights for the associated events gave the number of reactions of this type that occurred. The cross section was then obtained from the relation

$$\sigma(\bar{p}p \to n p \pi^-) = \frac{\sum_i W_i \cdot \sigma_t'(\bar{p}p)}{\text{total number of observable } \bar{p} \text{ interactions}} \quad . \qquad (18)$$

The annihilation cross section for the antineutrons determined by Eq. (13) with $a = 9.896$ was divided by K to obtain a cross section for annihilation into more than one prong. This corrected annihilation cross section was used by the WEIGHT program to determine the W_i for each of the 18 "good" events.

For the 18 events $\sum_{i=1} W_i = 205 \pm 50$, corrected for a combined scanning efficiency of 0.99. By use of Eq. (18) we obtained

$$\sigma(\bar{p} + p \to \bar{n} + p + \pi^- = 0.99 \pm .24 \text{ mb}.$$

In Table III the 20 antineutron stars associated with 2-prongs are broken down according to the classifications described in Section IV-A.

The center-of-mass angles between the antiproton and the other particles of the 2-prong interaction are plotted in Fig. 12 for the 20 events that fit the reaction. The antineutron tends to go forward and the proton backward, with the pion having roughly an isotropic distribution. The distribution of antineutron azimuthal angle about the $\bar{p}$ direction is plotted in Fig. 13. Zero azimuthal angle is defined by the direction of the proton. It is seen that the antineutron and proton tend to go in opposite directions transverse to the antiproton direction.

D. The Nature of the Antineutron Annihilation Stars

As was mentioned in Section IV-B, the ratio of the number of 5-prongs to 3-prongs was observed to be $R = 0.52 \pm .11$ for the events that had an antineutron kinetic energy between 800 and 1000 Mev. For all 142 stars (122 0-prong associations plus 20 2-prong associations), the ratio is $0.64 \pm .12$; the kinetic energy distribution for the antineutrons extends from 75 Mev to 1100 Mev (average, 765 Mev). This point is indicated in Fig. 6 by the symbol (A). Eighty percent of the 0-prong star associations had an antineutron kinetic energy between 800 and 1000 Mev. Since the ratio R is a function of energy, the ratio calculated for the 96 events in this energy range was thought to be the more realistic value.

The average charged-pion multiplicity for the 142 stars was $3.8 \pm .3$. If an additional 12% in the number of stars due to 1-prong annihilation is assumed to exist, the multiplicity becomes $3.5 \pm .3$. The statistical model predicts that the number of charged pions is about twice the number of neutral pions, which would then imply that the total pion multiplicity was $5.2 \pm .4$. The statistical model (see Appendix) predicts a multiplicity of 5.1 for $\lambda = 5$, and 5.3 for $\lambda = 6$.

The pion momentum distribution determined in the c.m. of the $\bar{n}$-p system is plotted for 3-prong stars in Fig. 14, and for 5-prong stars in Fig. 15, They are compared with the distribution predicted according to the statistical model for volume parameters $\lambda = 5$ and $\lambda = 6$. The areas of these curves are normalized to the numbers of pions plotted. Very good agreement is obtained for the 3-prong stars. Agreement is quite good for the 5-prong stars, but the observed distribution may peak at a slightly lower energy than that predicted. It should be noted that the momentum distribution is a relatively weak function of the statistical-model interaction volume.

The angle between the incoming antineutron direction and the pion direction in the c.m. frame of the $\bar{n}$-p system was calculated for each pion of the measurable events. The distribution of this angle was found to be, within statistics, an isotropic distribution (see Fig. 16).

To detect possible pion-pion correlations in the annihilations, the angle θ_{12} between pairs of pions was determined in the c.m. frame of the $\bar{n}$-p system for pairs with like and unlike charge. The number of pairs with pair angle θ_{12} less than 90 deg and the number with θ_{12} greater than 90 deg was then obtained. The ratios

$$\gamma = \frac{\text{number with } \theta_{12} > 90 \text{ deg}}{\text{number with } \theta_{12} < 90 \text{ deg}}$$

corresponding to these numbers are given in Table IV.

Although the errors are large, a smaller value for γ_ℓ than for γ_μ is clearly indicated. These ratios show that the angle between pions of like charge tends to be smaller than that between unlike pions. Similar results have been noted and discussed for antiproton-proton annihilations.[25,26] The like-pion correlations can be explained, in part, by the influence of Bose-Einstein statistics for pions of like charge.[26] The total wave function describing a particular state for an interaction containing like bosons is required to be unchanged upon interchange of the like bosons. If the state function used in the matrix element of the statistical model is made symmetric with respect to pairs of like pions, the predicted values for γ_ℓ and γ_μ are such that γ_μ is greater than γ_ℓ. In this model the correlations of like pions are due to the effect of the Bose-Einstein symmetrization, and do not consider any pion-pion interaction. This model is only partially successful, and requires a radius for the the interaction volume of three-quarters of a pion Compton wavelength. With this small radius, the model does not predict the observed pion multiplicity in annihilations.

The total energy of like and unlike pairs of pions was calculated in the c.m. frame of the two pions. The distribution of energies thus obtained appeared to peak at a slightly lower energy for like pairs than for unlike pairs; However, the statistics were poor owing to the small number of stars. This result is compatible with $\gamma_\ell < \gamma_\mu$ obtained above.

All the frames containing 3-, 5-, or 7-prong stars were scanned for a V pointing at the star. Only one event was found to fit a K^0 coming from a star, and this 3-prong star was not associated with either a 0- of 2-prong antineutron production. In addition, two V's were found that fitted a K^0 coming from a 1-prong annihilation. In one of these the antineutron came from a 2-prong, and in the other the antineutron was produced by a 0-prong. For the latter case the 1-prong and the 0-prong ending were only 2 deg apart as measured from the V. It was therefore uncertain whether the K^0 came from the 1-prong or was produced by the 0-prong. From these investigations it was possible only to say that K's are probably produced in $\bar{n}$-p annihilations, and that perhaps the K production in $\bar{n}$-p annihilation is less than that in $\bar{p}$-p annihilation.

V. DISCUSSION

The value obtained for the antineutron annihilation cross section at 900 Mev, $\sigma_{ann}(\bar{n}\text{-}p) = 45.2 \pm 5.4$ mb, agrees within statistics with the antiproton annihilation cross section,[27] $\sigma_{ann}(\bar{p}\text{-}p) = 51 \pm 3$ mb. The $\bar{p}$-p annihilation is composed of half isotopic singlet and half isotopic triplet states, while $\bar{n}$-p annihilation is a pure isotopic triplet state. The similarity of the annihilation cross sections indicates that the annihilation amplitudes for the singlet and triplet states are also similar.

It should be noted that an error occurs in the determination of $\sigma_{ann}(\bar{n}\text{-}p)$ in that the energy for the $\bar{n}$ was determined on the basis of Reaction (1), $\bar{p} + p \rightarrow \bar{n} + n$. It was estimated, however, that about 13% of the antineutrons were produced by Reaction (2), $\bar{p} + p \rightarrow \bar{n} + n + \pi^0$, and would therefore have a lower energy more in keeping with the energy distribution for $\bar{n}$'s produced in 2-prongs (see Fig. 11).

The values used for K, the correction for 1-prong annihilation, were calculated from the predictions of the statistical model for $\lambda = 5$. However, there is some indication that λ may be closer to 6. Fortunately, K is not a strong function of λ and decreases by only about 2% if λ is changed from 5 to 6. A more serious question is whether the statistical-model prediction of 12% for the 1-prong annihilation is in error.

An analysis of the ratio of the number of 2-, 4-, and 6-prongs in $\bar{p}$-p annihilation also gives a fit to the statistical-model predictions for a λ of about 5 or 6.[27]

The total inelastic cross section for antiprotons on neutrons[7] is $\sigma_i(\bar{p}\text{-}n) = 65 \pm 4$ mb at 900 Mev. Since this is in a pure isotopic triplet state also, it should be the same as the inelastic $\bar{n}$-p cross section. Assuming this to be so implies that the inelastic $\bar{n}$-p cross section not due to annihilation

is 20 ± 7 mb. The proton-proton interaction is also a pure isotopic triplet state, and its inelastic cross section at 900 Mev is about 25 ± 5 mb.[28]

The total charge exchange cross section $\sigma_{ce} = 7.8 \pm .6$ mb is in agreement with previous results.[3,4] This result contains an inelastic part due to Reaction (2), which, from statistical-model arguments, was estimated to be about 1 mb. The angular differential cross section for charge exchange, $d\sigma_{ce}/d\Omega$, plotted in Fig. 9, also contains this 13% inelastic contamination. The inelastic differential cross section is probably similar to that for Reaction (3), $\bar{p} + p \rightarrow \bar{n} + p + \pi^-$, which is not peaked as strongly in the forward direction (see Fig. 12).

In four events of the 0-prong $\bar{n}$ production, the antineutron came off backward in the center-of-mass frame (see Fig. 9). Since there are estimated to be 5 or 6 false associations, some or all of the backward events may be false. However, the angular distribution for the false associations is expected to be isotropic. Therefore, at least some of these backward events are believed to be real associations, but may be due to Reaction (2), the inelastic charge-exchange mode. Note that in two cases the $\bar{n}$ went backward for Reaction (3) (see Fig. 12).

On the basis of the statistical model, 2% of the antiproton-proton annihilations should be 0-prong annihilations. From the total number of antiproton interactions, 18,728, and the annihilation and total $\bar{p}$-p cross sections, the predicted number of 0-prong $\bar{p}$-p annihilations was 212 ± 15. The number of 0-prong $\bar{p}$ annihilations determined from the number of electron-positron pairs (Section III-D-1) was 61 ± 54. There apparently is disagreement here with the statistical model predictions for the fraction of annihilations producing all π^0's.[29]

ACKNOWLEDGMENTS

We wish to thank the many people of the Lawrence Radiation Laboratory who have aided in the above work. Dr. Sherwood Parker was in charge of the spectrometer alignment, and Mr. Jim Carroll helped with the operation of the electronics and the preliminary data analysis.

The experimental setup was under the direction of Dr. M. Lynn Stevenson of Dr. Alvarez's group. Donald Gow headed the group operating the bubble chamber, and Dr. Edward Lofgren, the group operating the Bevatron. The accelerator technicians under Don Bliss constructed the counters, and Dick Mack and Horace Jackson of the counter development group aided in designing and maintaining some of the special electronic equipment. Finally, there were many film scanners and measurers and IBM 704 programmers who helped in the data reduction. To all these people we express our sincere thanks.

APPENDIX

Statistical-Model Predictions

Several calcualtions[30 - 36] have been made of the pion multiplicity in nucleon-antinucleon annihilation according to the Fermi statistical model. The original form for the phase space associated with each pion, $\Omega d^3\vec{p}$, suggested by Fermi,[30] was not Lorentz-invariant. Numerical evaluation of the phase-space integrals, however, can be greatly simplified if the covariant form $\frac{\mu\Omega}{\omega} d^3\vec{p}$ is used.[33 - 36] Here Ω, ω, p, and μ are, respectively, the interaction volume, energy, momentum, and mass of the pion. This modification seems plausible on the basis of field theory. This covariant form is actually the expression obtained from the covariant S-matrix theory if it is assumed that the S matrix for the emission of n pions is independent of the energies and momenta of the emitted pions. In view of the crude nature of the Fermi model, such a simple modification may not be unreasonable. For these reasons the covariant form for the phase space was used.

With no consideration of selection rules and assuming that the matrix element for nucleon-antinucleon annihilation is constant, one obtains, for the transition probability for a state of n pions in an isotopic spin state I,

$$S_n(I) = A \frac{G(I)}{n!} \frac{(\mu\Omega)^n}{(2\pi)^{3n}} T_n(E) . \qquad (A-1)$$

Here $\hbar = c = 1$, G(I) is the isotopic spin weight factor, A is a constant independent of n, and $T_n(E)$ is the covariant phase-space integral in the center-of-mass frame at total energy E.

$$T_n(E) = \int \prod_{i=1}^{n} \frac{d^3\vec{p}_i}{\omega_i} \delta\left(E - \sum_{i=1}^{n} \omega_i\right) \delta\left(\sum_{i=1}^{n} \vec{p}_i\right) . \qquad (A-2)$$

For a particular n and E the only variable parameter in $S_n(I)$ is Ω, the interaction volume. Convenient variation of this parameter was achieved by setting $\Omega = \lambda \Omega_0$, where $\Omega_0 = \frac{4}{3}\pi \frac{1}{\mu^3}$, ($\hbar = c = 1$). Thus Ω_0 is the volume of a sphere with a radius of one pion Compton wave length.

Equation (A-2) can be written

$$T_n(E) = 4\pi \int p_1 \, d\omega_1 \left[\int \prod_{i=2}^{n} \frac{d^3\vec{p}_i}{\omega_i} \, \delta\left(E - \omega_1 - \sum_{i=2}^{n} \omega_i \right) \delta\left(\vec{p}_1 + \sum_{i=2}^{n} \vec{p}_i \right) \right], \quad \text{(A-3)}$$

where $d^3\vec{p} = 4\pi p^2 \, dp = \omega p \, d\omega$.

Since $d^3\vec{p}/\omega$ is Lorentz-invariant, the square bracket in the Lorentz frame where

$$\sum_{i=2}^{n} \vec{p}_i = 0 \quad \text{and} \quad \sum_{i=2}^{n} \omega_i' = E' \text{ becomes}$$

$$\left[\int \prod_{i=2}^{n} \frac{d^3\vec{p}_i'}{\omega_i'} \, \delta\left(E' - \sum_{i=2}^{n} \omega_i' \right) \delta\left(\sum_{i=2}^{n} \vec{p}_i' \right) \right], \quad \text{(A-4)}$$

which is just $T_{n-1}(E')$ according to Eq. (A-2). Hence, the recursion relation is

$$T_n(E) = 4\pi \int_{\mu}^{\bar{\omega}_1} p_1 \, d\omega_1 \, T_{n-1}(E'). \quad \text{(A-5)}$$

From Lorentz invariance, $\left(\sum_{i-2}^{n} \omega_1 \right)^2 - \left(\sum_{i=2}^{n} \vec{p}_i \right)^2$ = constant in all coordinate systems. Thus we have $(E')^2 - 0 = (E-\omega_1)^2 - p_1^2$, defining E'. The maximum energy $\bar{\omega}_1$ assumed by particle 1 corresponds to $E' = (n-1)\mu$.

The upper limit to the integral in Eq. (A-5) is then $\bar{\omega}_1 = \frac{E^2 - n(n-2)\mu}{2E}$. By means of Eq. (A-5), $T_n(E)$ can be evaluated successively, where finally

$$T_2(E) = 2\pi(1 - 4\mu^2/E^2)^{1/2} . \qquad (A-6)$$

Thus for a particular energy E and volume factor λ the relative probabilities for producing various numbers of pions can be calculated.

If it is assumed that all individual channels contribute, with the same weight, to the total transition probability, the branching ratios for the various modes can be calculated for each number of pions emitted. For example, in the case in which $n = 3$, there are two modes of antineutron-proton annihilation:

$$\bar{n} + p \rightarrow 2\pi^0 + \pi^+,$$

$$\bar{n} + p \rightarrow 2\pi^+ + \pi^-.$$

The branching ratios have been calculated by Pais[37] as 2/5 and 3/5, respectively.

The values of $T_n(E)$ calculated by Desai[35] and the branching ratios evaluated by Pais[37] were used to calculate the fraction of annihilations occurring by each mode, for values of n up to $n = 8$ and for various values of λ and E. (The annihilations with n greater than 8 is less than 1% for the energies considered.) These calculations were performed by an IBM 650 program called PASBAR. This program also determined the average pion multiplicity, the ratio of the number of charged pions to neutral pions, and the fraction of annihilations giving 1-, 3-, 5-, and 7-prongs (a 1-prong corresponds to one charged pion, a π^+). In addition, the number

$$K(E) = \frac{1}{\text{fraction of } 3 + 5 + 7 \text{ prongs}} , \qquad (A-7)$$

which is the correction for unobservable 1-prong annihilations, was also calculated. In Fig. 7 K is plotted as a function of antineutron laboratory-frame kinetic energy for $\lambda = 5$.

The ratio of the number of 5-prong to 3-prong annihilations as a function of antineutron laboratory-frame kinetic energy is plotted in Fig. 6 for various values of λ.

The momentum distribution for one of the pions in an annihilation producing n pions can be obtained by simply not performing the first integral in Eq. (A-3),

$$\frac{dT_n(E)}{dp_1} = 4\pi \frac{p_1^2}{\omega_1}\left[\int \prod_{i=2}^{n} \frac{d^3\vec{p}_i}{\omega_i}\, \delta\left(E-\omega_1 - \sum_{i=2}^{n}\omega_i\right)\, \delta\left(\vec{p}_1 + \sum_{i=2}^{n}\vec{p}_i\right)\right]. \qquad (A-8)$$

From Eqs. (A-1) and (A-8), $\frac{dS_n(E)}{dp_1}$ can be obtained. The momentum distribution for pions in a 3-prong annihilation is then given by

$$\frac{dS_{3PR}}{dp_1} = \sum_n f_{3,n}\, \frac{dS_n(E)}{dp_1}\ , \qquad (A-9)$$

where $f_{3,n}$ is the fraction of the n pion annihilations giving 3-prong stars. A similar relation gives the momentum distribution of pions in 5-prong annihilations:

$$\frac{dS_{5PR}}{dp_1} = \sum_n f_{5,n}\, \frac{dS_n(E)}{dp_1}\ . \qquad (A-10)$$

The $f_{3,n}$ and $f_{5,n}$ are determined from the PASBAR output.

Equation (A-8) was evaluated for values of n up to n = 8 by an IBM 709 program which used the Monte Carlo method to evaluate the integrals. (A normal numerical integration for the larger n values would have required too much computer time.)

Momentum distributions thus calculated, for $\lambda = 5$ and $\lambda = 6$ and an antineutron lab kinetic energy of 900 Mev, are given in Figs. 14 and 15, for 3-prong and 5-prong annihilations, respectively. The curves have been normalized to the numbers of pions observed.

FOOTNOTES AND REFERENCES

* Work done under the auspices of the U.S. Atomic Energy Commission.

† Present address: Aerojet General Nucleonics, San Ramon, California.

1. B. Cork, G. R. Lambertson, O. Piccioni, and W. A. Wenzel, Phys. Rev. 104, 1193 (1956).

2. C. A. Coombes, B. Cork, W. Galbraith, G. R. Lambertson, and W. A. Wenzel, Phys. Rev. 112, 1303 (1958).

3. T. Elioff, L. Agnew, O. Chamberlain, H. M. Steiner, C. Wiegand, and T. Ypsilantis, Phys. Rev. Letters 3, 285 (1959).

4. R. Armenteros, C. A. Coombes B. Cork, G. R. Lambertson, and W. A. Wenzel, Phys. Rev. 119, 2068 (1960).

5. J. Button, T. Elioff, E. Segrè, H. M. Steiner, R. Weingart, C. Wiegand, and T. Ypsilantis, Phys. Rev. 108, 1557 (1957).

6. L. E. Agnew, Jr., T. Elioff, W. B. Fowler, L. Gilly, R. L. Lander, L. Oswald, W. M. Powell, E. Segrè, H. Steiner, H. White, C. Wiegand, and T. Ypsilantis, Phys. Rev. 110, 994 (1958); L. E. Agnew, Jr., T. Elioff, W. B. Fowler, R. L. Lander, W. M. Powell, E. Segrè, H. M. Steiner, H. S. White, C. Wiegand, and T. Ypsilantis, Phys. Rev. 118, 1371 (1960).

7. T. Elioff, Antiproton-Nucleon Cross Sections from 0.5 to 1.0 Bev (Thesis), Phys. Rev. (to be published) (Lawrence Radiation Laboratory Report UCRL-9288, July 1960).

8. M. Lynn Stevenson, in 1959 Kiev Conference on High Energy Physics (to be published).

9. J. Button, P. Eberhard, G. R. Kalbfleisch, J. E. Lannutti, G. R. Lynch, B. C. Maglić, M. L. Stevenson, and N. H. Xuong, Phys, Rev. 121, 1788 (1961).

10. P. Eberhard, R. H. Good, and H. K. Ticho, A Separated 1.17-Bev/c K^--Meson Beam, Rev. Sci. Instr. 31, 1054 (1960).

11. H. K. Ticho, The Production, Transport, and Separation of Beams, in Proceedings of the International Conference on High Energy Accelerators and Instrumentation (CERN, Geneva, 1959), pp. 387-396. A brief description of the parallel-plate velocity spectrometer is also given in Ref. 2.

12. J. D. Gow and A. H. Rosenfeld, Berkeley 72-Inch Hydrogen Bubble Chamber, in Proceedings of the International Conference on High Energy Accelerators and Instrumentation (CERN, Geneva, 1959), pp. 435-439.

13. The Franckenstein measuring projector was designed and built by Jack V. Franck and his group. A brief description of this machine is contained in the second item of Ref. 14.

14. Developed by Frank T. Solmitz, R. Harvey, and W. Humphrey; A description of the PANG program, Alvarez Group Memo 111, Sept. 18, 1959, and Memo 115, Oct. 25, 1959, Lawrence Radiation Laboratory; A. H. Rosenfeld, Digital Computer Analysis of Data from Hydrogen Bubble Chambers at Berkeley, in Proceedings of the International Conference on High Energy Accelerators and Instrumentation (CERN, Geneva, 1959), pp. 533-539.

15. B. Rossi, High Energy Particles (Prentice-Hall, Inc., New York, 1952), p. 14.

16. It is seen in Fig. 4 that the average pion momentum is about 1.5 Bev/c, and is lower than the average antiproton momentum.

17. B. Rossi, High Energy Particles (Prentice-Hall, Inc., New York, 1952), p. 16.

18. T. J. Devlin, B. C. Barish, W. N. Hess, V. Perez-Mendez, and J. Solomon, Phys. Rev. Letters 4,242 (1960).

19. P. Falk-Vairant and G. Valladas, Results in Pion-Proton Scattering Near the Higher Resonances, in Proceedings of the 1960 Annual International Conference on High Energy Physics at Rochester (Interscience Publishers, Inc., New York, 1960), pp. 38-45; J. C. Brisson, P. Falk-Vairant, J. P. Merlo, P. Sonderegger, R. Turlay, and G. Valladas, Measurement of the Total Cross Section for π^--p Charge Exchange from $T_\pi = 0.4$ Gev to $T_\pi = 1.5$ Gev, in Proceedings of the 1960 Annual International Conference on High-Energy Physics at Rochester (Interscience Publishers, Incl., New York, 1960),, pp. 191-193.

20. This was obtained by extrapolating the curves for the cross section of the reactions $\pi^- + p \rightarrow \pi^0 + n$ and $\pi^- + p \rightarrow 2\pi^0 + n$, with the sum of the cross sections equal to 4.75 mb. The curves were taken from a preprint furnished by P. Falk-Vairant, and will appear in the Proceedings of the Strong Interaction Conference at Berkeley, December 1960. See also Ref. 19.

21. The cross section for the reactions $\bar{p} + p \rightarrow n + \bar{p} + \pi^+$ and $\bar{p} + p \rightarrow \bar{p} + p + \pi^0$ were obtained by private communication from Gerald R. Lynch (Lawrence Radiation Laboratory) (to be published in Phys. Rev.).

22. This estimate of the number of events for Reaction (2) may be somewhat low. The ratio of the cross section for Reaction (2) to that for Reaction (3) is predicted to be 4/5 by the statistical model; however, the isobar model predicts a ratio of 2 [see S. J. Lindenbaum and R. M. Sternheimer, Phys. Rev. Letters 5, 24 (1960)]. Recent experimental results for the reaction $\bar{p} + p \rightarrow \bar{p} + p + \pi^0$ give a cross section of $1.6 \pm .3$ mb (see Ref. 21), which should be the same as that for Reaction (2). The effect of increasing the ratio of Reaction (2) to (3) is to reduce $N_{0\,\bar{p}\,\mathrm{ann.}}$

23. Z. Koba and G. Takeda, Progr. Theoret, Phys. (Kyoto) 19, 269 (1958).

24. Originally developed by A. Rosenfeld, J. Snyder, and J.P. Berge for treatment of K-meson interactions. A. H. Rosenfeld and J. N. Snyder, Digital Computer Analysis of Data from Bubble Chambers. IV. The Kinematic Analysis of Complete Events, Rev. Sci. Instr. (to be published) (Lawrence Radiation Laboratory Report UCRL-9098, Feb. 1960); J. P. Berge, F. T. Solmitz, and H. Taft, Digital Computer Analysis of Data from Bubble Chambers. III. The Kinematical Analysis of Interaction Vertices, Rev. Sci. Instr. (to be published) (Lawrence Radiation Laboratory Report UCRL-9097, March 1960).

25. G. Goldhaber, W. Fowler, S. Goldhaber, T. Hoang, T. Kalogeropoulos, and W. Powell, Phys. Rev. Letters 3, 181 (1959).

26. G. Goldhaber, S. Goldhaber, W. Lee, and A. Pais, Phys. Rev. 120, 300 (1960).

27. Gerald R. Lynch (Lawrence Radiation Laboratory), private communication (to be published in Revs. Modern Phys.).

28. W. N. Hess, Revs. Modern Phys. 30, 368 (1958).

29. If the statistical-model predictions for $N_{0\,\bar{p}\,ann}$ is used in Eq. (12), $N_0^{\bar{n}}$ is reduced to 1473. The core radius a then becomes 0.959 fermi, which gives an antineutron annihilation cross section at 900 Mev of $\sigma_a(\bar{n}p) = 50$ mb. The charge-exchange cross sections become σ_{ce}(0-prong) = 7.1 mb; $\sigma(\bar{p} + p \rightarrow \bar{n} + p + \pi^-) = 0.9$ mb.

30. E. Fermi, Progr. Theoret. Phys. (Kyoto) 5, 570 (1950).

31. S. Z. Belenkii and I. S. Rosenthal, J. Exptl. Theoret. Phys. (USSR) 3,786 (1956).

32. G. Sudarshan, Phys. Rev. 103, 777 (1956).

33. P. P. Srivastava and G. Sudarshan, Phys. Rev. 110, 765 (1958).

34. M. Neuman, Statistical Models for High Energy Nuclear Reactions I and II, Separate Do Vol. 31, No. 3 and No. 4, Anais de Academia Brasileira De Ciencias, Rio de Janeiro, 1959.

35. B. R. Desai, Phys. Rev. 119, 1390 (1960).

36. T. E. Kalogeropoulos, A Study of the Antiproton Annihilation Process in Complex Nuclei (Thesis) Lawrence Radiation Laboratory Report UCRL-8677, March 1959 (unpublished).

37. A. Pais, Ann. Phys. 9, 548 (1960).

Table I. Summary of beam characteristics.

Energy of protons incident on the Bevatron target		6.2 Bev
Aluminum Bevatron target		
Size		5 in. azimuthally
		1/2 in. radially
		1/8 in. vertically
Physical position	Radius to outside edge	599.4 in.
	Azimuth (NW quadrant measured from west tangent tank)	22.34 deg
	Distance from Q 1 entrance	190 in.
Virtual position	(Distance from principal plane of Q 1)	
	Horizontally	600 in.
	Vertically	230 in.
Antiproton beam		
Momentum at target		1.64 Bev/c
Production angle (relative to internal proton beam)		1 ± 1 deg
Solid angle accepted		0.20 msr
Transmission of total system		0.33
Momentum (center of bubble chamber)		1.62 Bev/c
Momentum bite (at bubble chamber)		± 0.02 Bev/c
Average $\bar{p}$ flux per picture		1.1

Table I (cont'd)

Separation	
Spectrometer characteristics	
Plate length	19 ft
Width of uniform field	6 in.
Plate spacing	2-1/2 in.
Average operating voltage	385 kv
Average angular separation	3.1 mrad
Image widths W (vertical) at slits (1st/2nd/3rd systems)	0.20/0.18/0.4 in.[a]
Magnification (vertical) per stage	1.2/1.0/1.0
Spatial separation S of image per stage (at slits)	0.5/0.40/0.40 in.
W/S	0.40/0.45/1.0[a]
Pion/antiproton ratios at target	20,000/1
Pion/antiproton ratios at 72-in. bubble chamber	0.40/1
Rejection ratios for pions	
System 1	50
System 2	100
System 3	10[a]
Total	5×10^{4} [b]

Table I (cont'd)

Beam Composition and Total Flux	
Average beam composition at bubble chamber ($\bar{p}/\pi^-/\mu^-/K^-$)	1.0/0.40/2.7/0.002
Total number of antiprotons through chamber	46,800
Number of antiproton interactions	18,900

[a] At the conclusion of the 1.65-Bev/c run, it was found that Q5 had a misplaced pole tip, which accounted for the poor image width at Slit 3.

[b] This rejection ratio is based on all visible pion background in the chamber. Much of the pion background actually has a lower momentum than the antiproton beam proper. See Fig. 4.

Table II. Classification as to reliability of stars associated with 0-prongs.

Classification/event type	(0,3)	(0,5)	(0,7)	
I	21[a]	35	1	U^{vis}_{min} >1 Bev
II	9			U^{vis}_{min} >KE (neutron)
III	45	3		U^{vis}_{min} and momentum unbalance >1 Bev
IV	2	6[b]	1	unmeasurable
	77	44	1	Total = 122

[a] Includes one uncertain event described in text.

[b] Although the star could not be measured on the six events, it was possible to measure the 0-prong and the antineutron direction on three events.

Table III. Classification of stars associated with 2-prongs.

Classification/event type[a]	(2, 3)	(2, 5)	(2, 7)	
I	4	9	2	U_{min}^{vis} > 1 Bev
II	2			U_{min}^{vis} > KE (neutron)
III	2			U_{min}^{vis} and momentum unbalance ≥ 1 Bev
IV	—	1	—	unmeasurable
	8	10	2	Total 20

[a]Here the event type (2, 3) indicates a 3-prong star associated with a 2-prong, etc.

Table IV. The ratio γ_ℓ for like, and γ_μ for unlike, pairs of pions or pions in annihilation stars

3-prong stars	like	$(\pi^+ - \pi^+)$	$\gamma_\ell = 1.74 \pm 0.43$
	unlike	$(\pi^+ - \pi^-)$	$\gamma_\mu = 2.02 \pm 0.36$
5-prong stars	like	$(\pi^+ - \pi^+)$	$\gamma_\ell^+ = 0.87 \pm 0.16$
	like	$(\pi^- - \pi^-)$	$\gamma_\ell^- = 1.0 \pm 0.33$
	like	$(\pi^+ - \pi^+)$ plus $(\pi^- - \pi^-)$	$\gamma_\ell = 0.90 \pm 0.15$
	unlike	$(\pi^+ - \pi^-)$	$\gamma_\mu = 2.21 \pm 0.32$
3-prong plus 5-prong stars	like	$(\pi^+ - \pi^+)$ plus $(\pi^- - \pi^-)$	$\gamma_\ell = 1.11 \pm 0.15$
	unlike	$(\pi^+ - \pi^-)$	$\gamma_\mu = 2.13 \pm 0.24$

Figure Legends

Fig. 1. Plan view of experimental arrangement.

Fig. 2. Bubble chamber photograph of an antiproton charge exchange into an antineutron. The antineutron then annihilated into five charged pions.

Fig. 3. Bubble chamber photograph of the reaction $\bar{p} + p \rightarrow \bar{n} + p + \pi^-$. The $\bar{n}$ then annihilated into three charged pions (arrow).

Fig. 4. Momentum distribution for antiprotons and π^- mesons.

Fig. 5. Energy distribution of antineutrons produced by 0-prong charge exchange (117 events).

Fig. 6. Statistical-model predictions for the ratio R of the number of 5-prong to 3-prong annihilation stars.

Fig. 7. The correction factor for 1-prong annihilations, K, as a function of antineutron kinetic energy. $\lambda = 5$.

Fig. 8. The number of antineutrons produced by 0-pronngs, $N_0^{\bar{n}}$, as a function of the core radius, a.

Fig. 9. Differential cross section for charge exchange as a function of $\cos \Theta_{\bar{n},\bar{p}}^{c.m.}$, and angular distribution of the 117 events.

Fig. 10. χ^2 distribution for events to fit the reaction $\bar{p} + p \rightarrow \bar{n} + p + \pi^-$ (70 events).

Fig. 11. Energy distribution of antineutrons produced by 2-prong charge exchange (19 events).

Fig. 12. Center-of-mass angular distribution of the particles in the reaction $\bar{p} + p \rightarrow \bar{n} + p + \pi^-$ relative to the $\bar{p}$ direction (20 events).

Fig. 13. Azimuthal angular distribution of the $\bar{n}$ about the $\bar{p}$ direction in the reaction $\bar{p} + p \rightarrow \bar{n} + p + \pi^-$ (20 events). Zero azimuthal angle is defined by the direction of the proton.

Fig. 14. Center-of-mass momentum distribution of charged pions in 3-prong annihilation stars.

Fig. 15. Center-of-mass momentum distribution of charged pions in 5-prong annihilation stars.

Fig. 16. Distribution of the number of charged pions as a function of $\cos\Theta^{c.m.}_{\pi^{\pm}, \bar{n}}$. (Includes 3-, 5-, and 7- prong stars.)

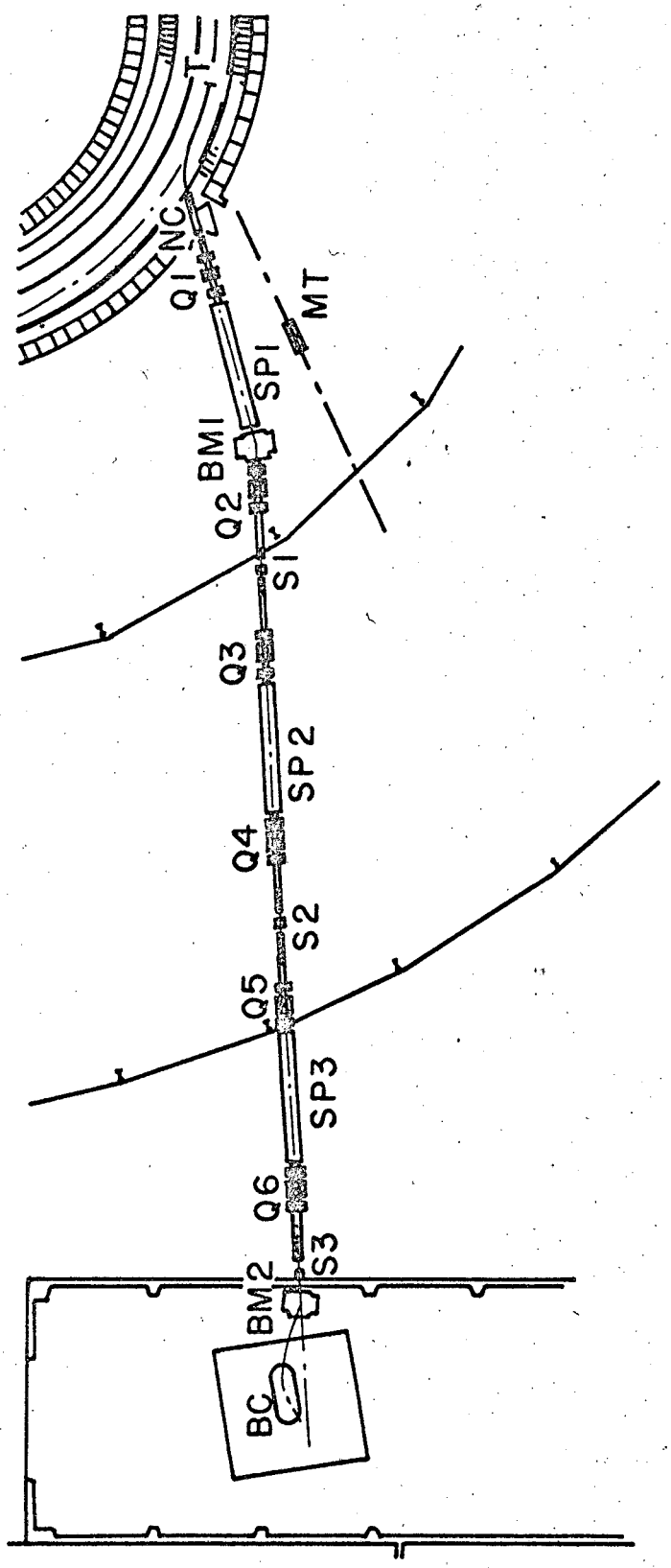

MU-21076-A

Fig. 1.

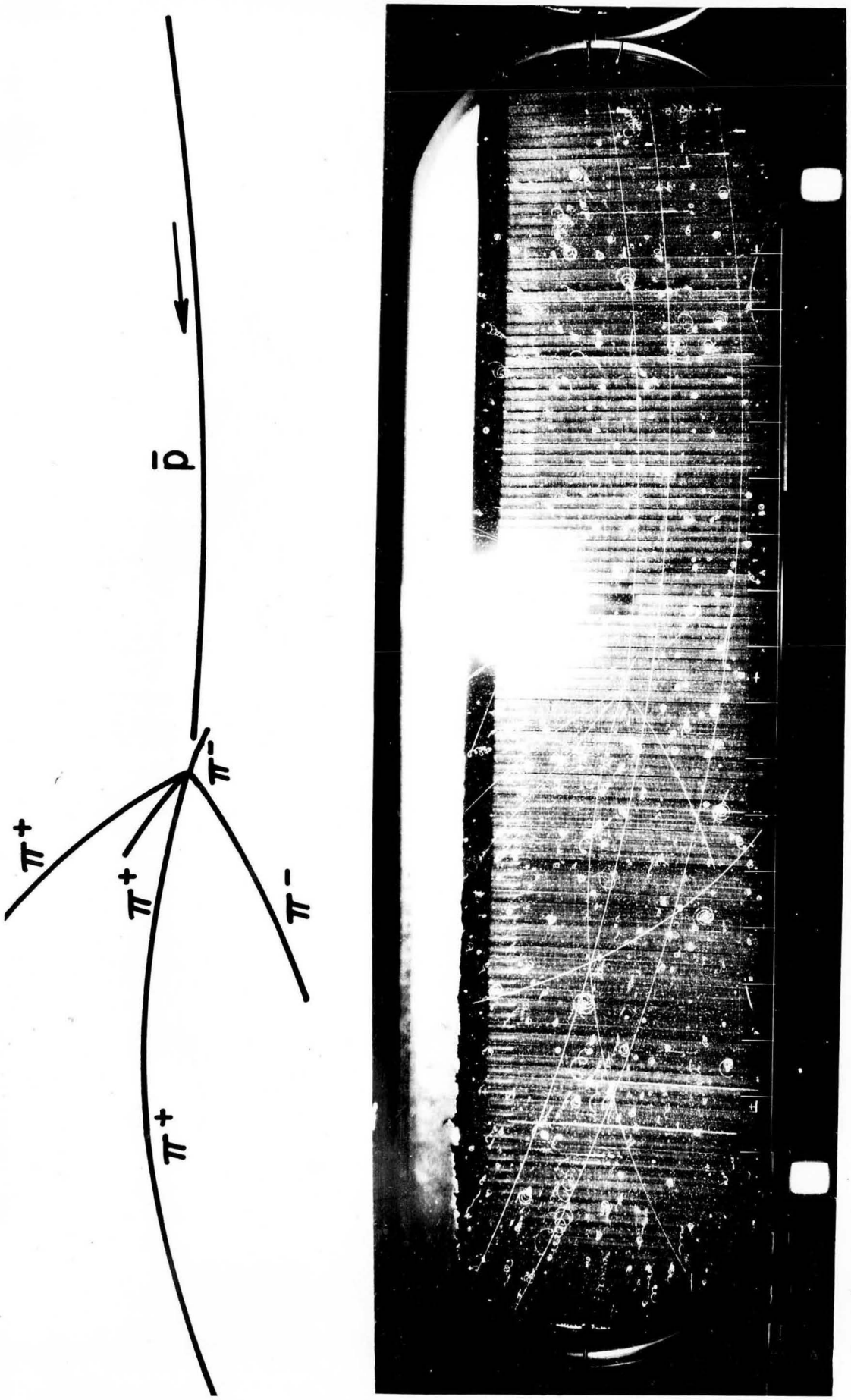

Fig. 2.

Fig. 3.

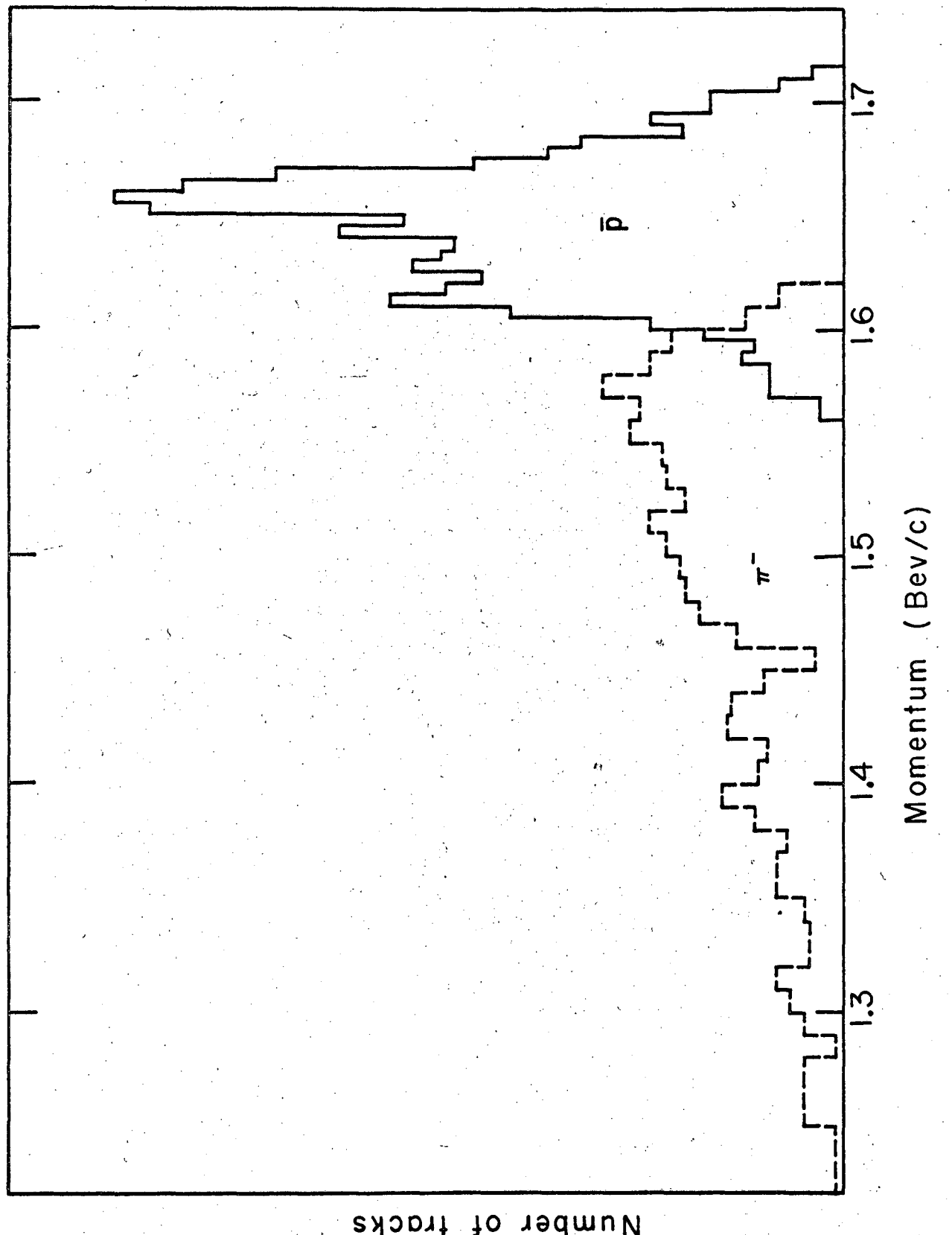

Fig. 4.

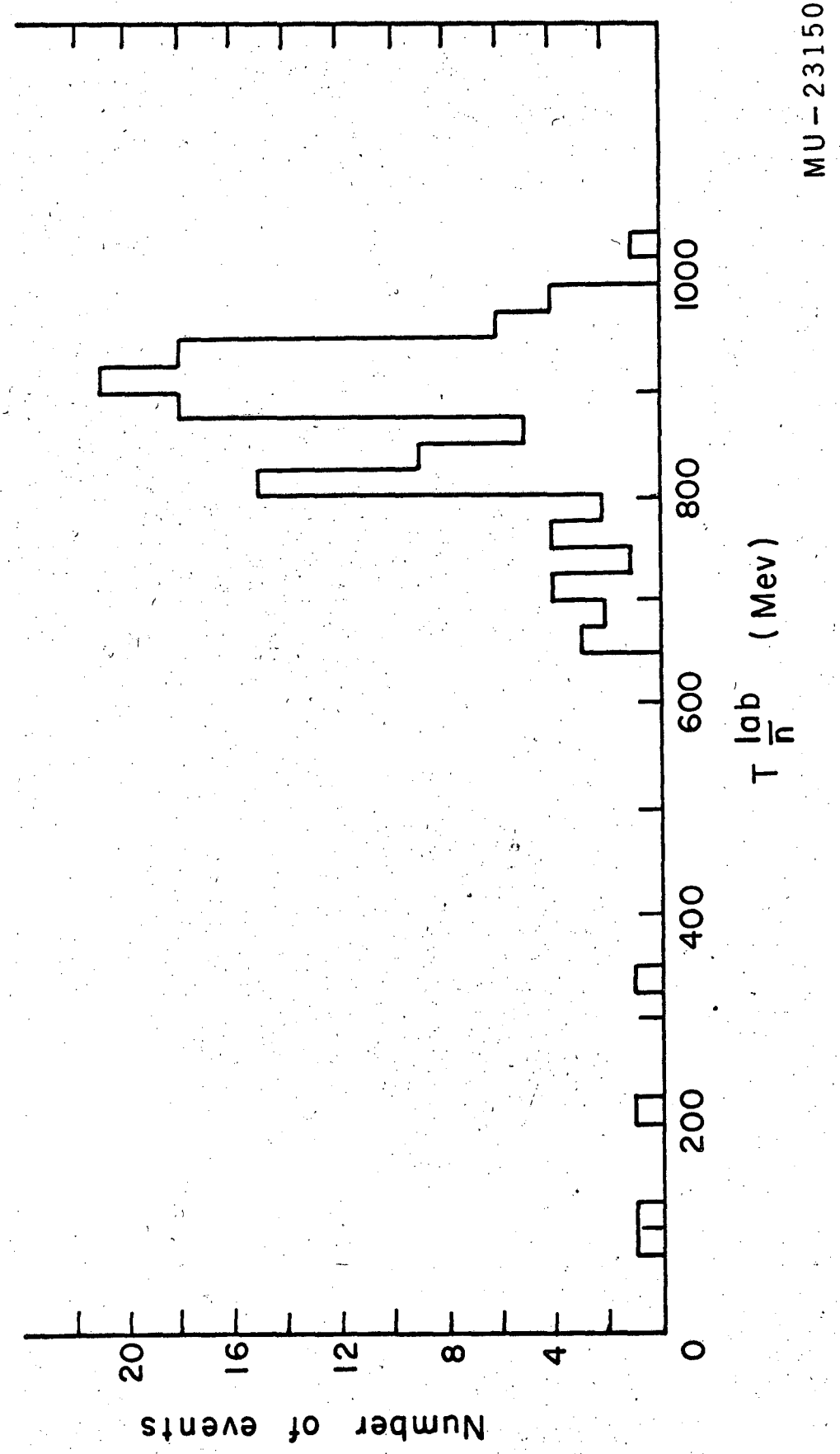
MU-23150
Number of events
0
4
8
12
16
20
200
400
600
800
1000
$T_{\frac{lab}{n}}$ (Mev)

Fig. 5.

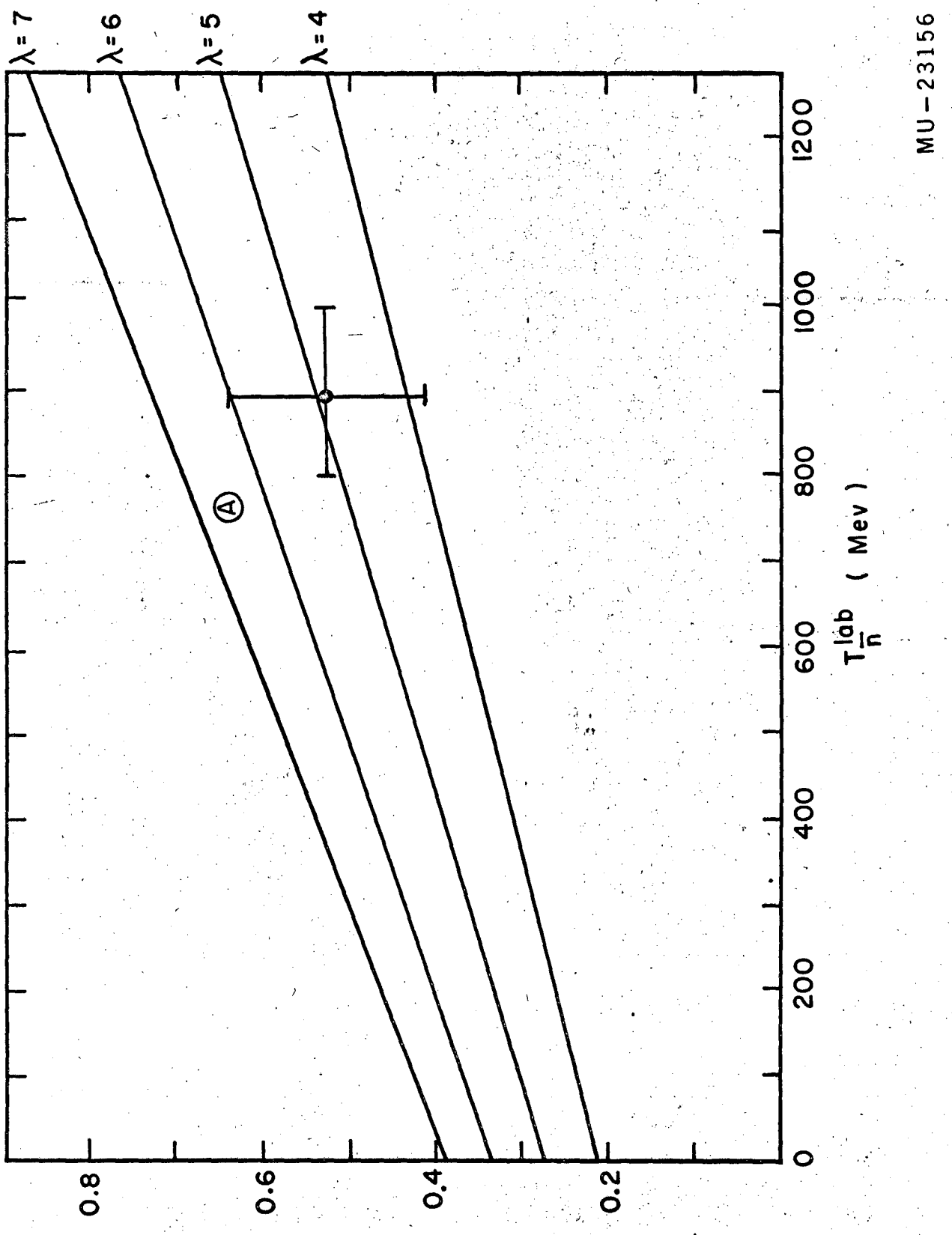
λ=7
λ=6
λ=5
λ=4
Ⓐ
0.8
0.6
0.4
0.2
Ratio, R
0
200
400
600
800
1000
1200
$T_{\bar{n}}^{lab}$ (Mev)
MU-23156

Fig. 6.

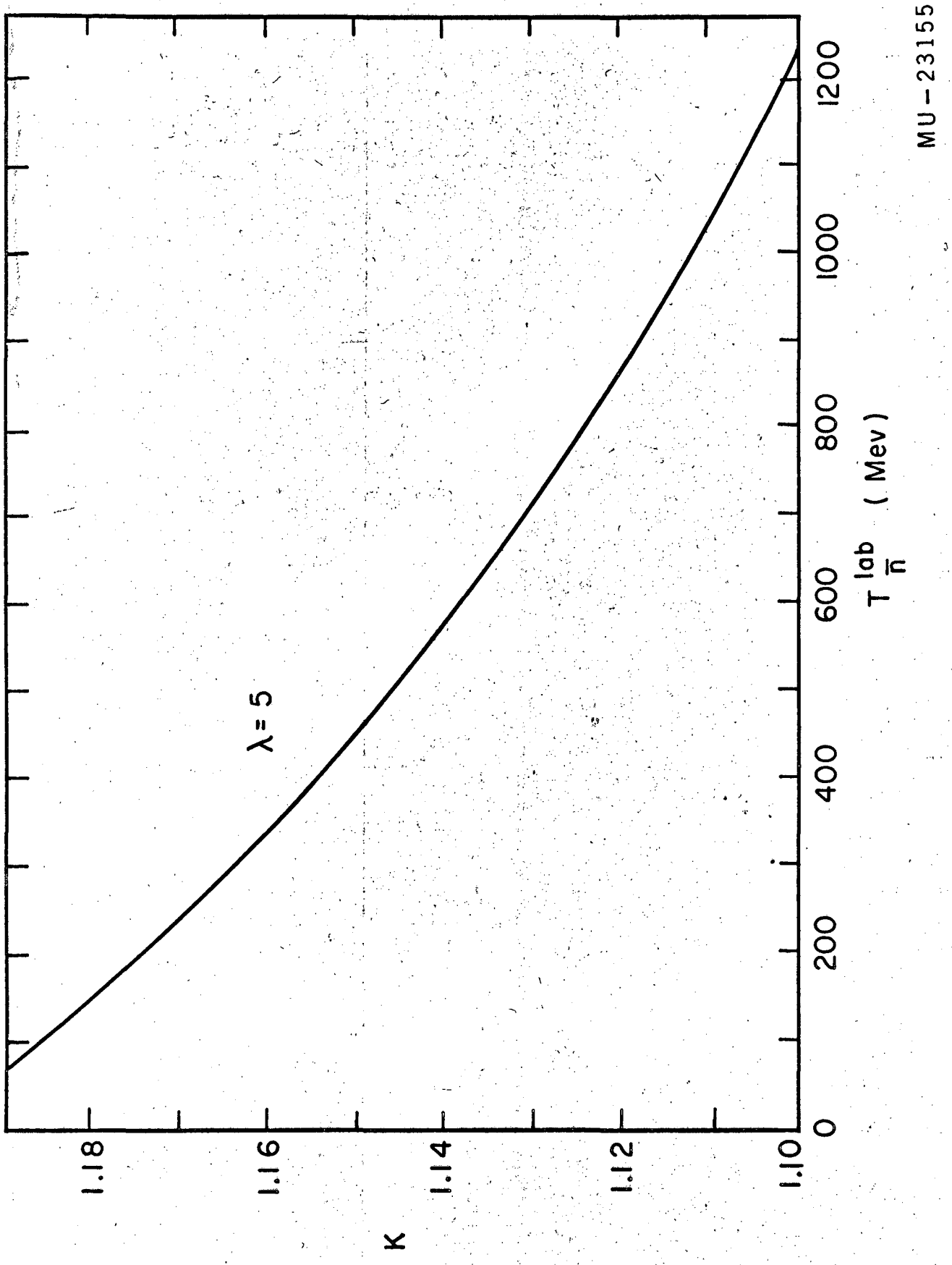
MU-23155
λ=5
K
1.10
1.12
1.14
1.16
1.18
0
200
400
600
800
1000
1200
$T_{\bar{n}}^{lab}$ (Mev)

Fig. 7

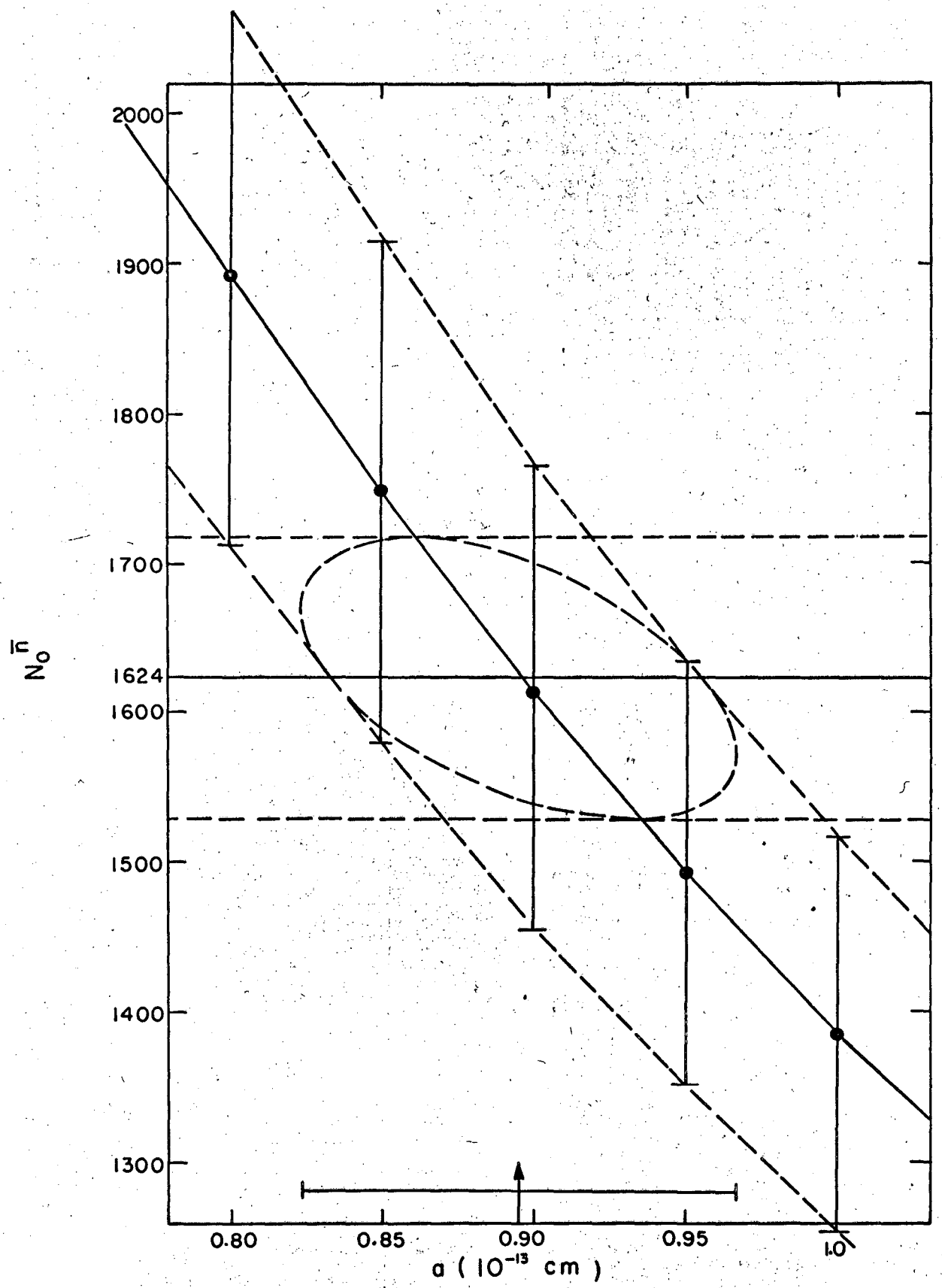
2000
1900
1800
1700
1624
1600
1500
1400
1300
$\overline{n}$
N_0
0.80
0.85
0.90
0.95
1.0
a (10^{-13} cm)
MU-23161

Fig. 8

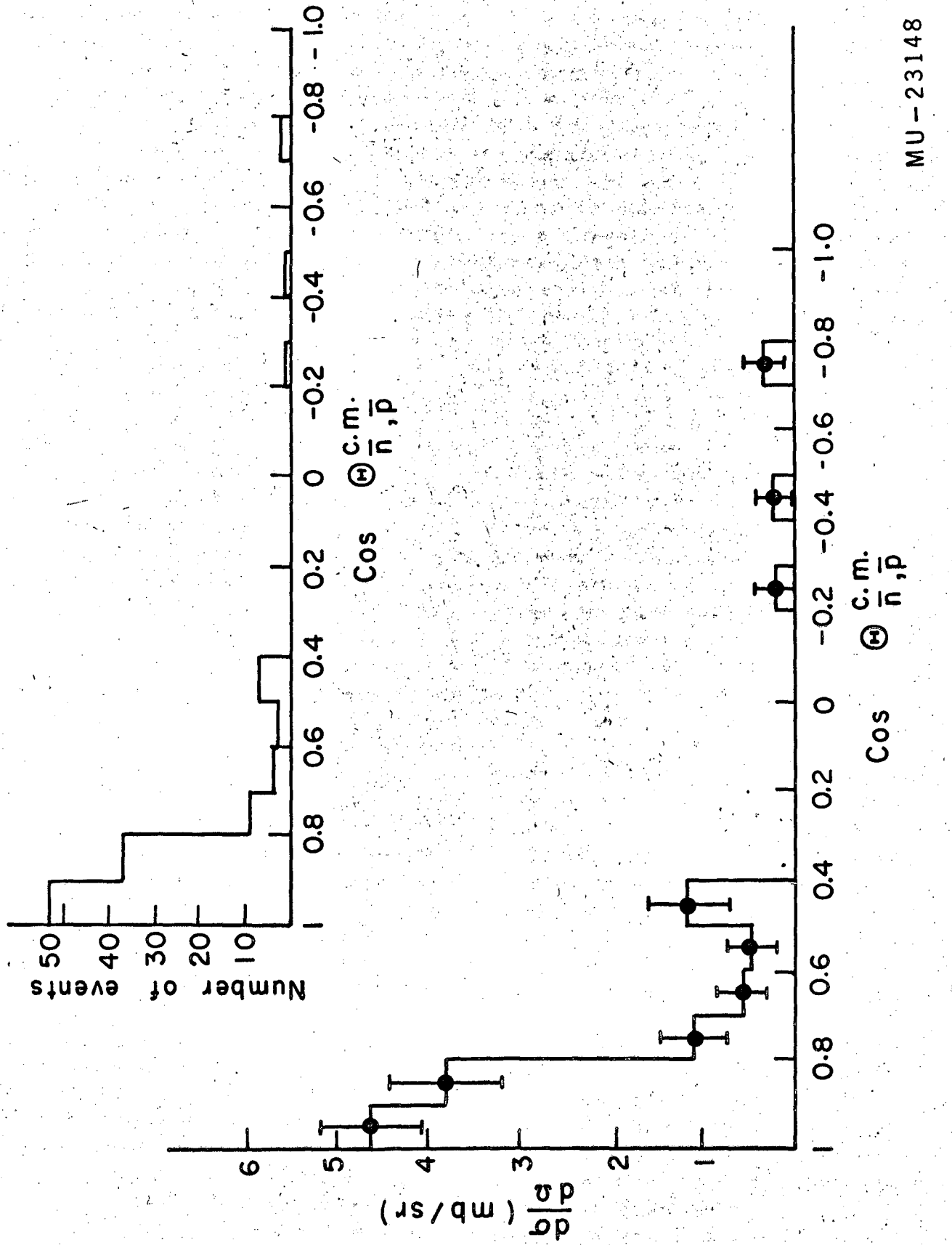
MU-23148
$\frac{d\sigma}{d\Omega}$ (mb/sr)
Cos Θ c.m. $\bar{n}, \bar{p}$
Number of events
Cos Θ c.m. $\bar{n}, \bar{p}$

Fig. 9

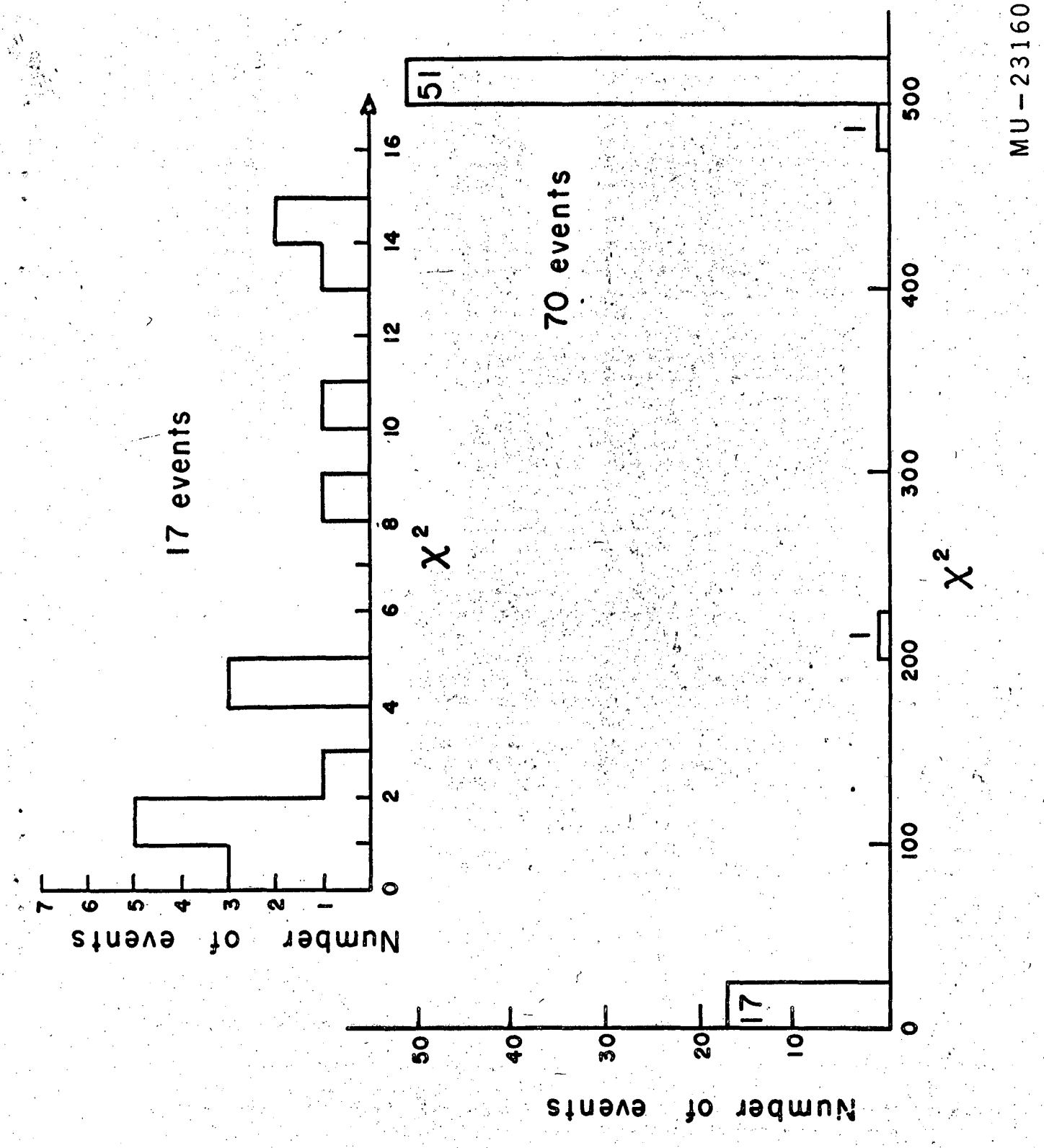
17 events
Number of events
χ²
70 events
Number of events
χ²
MU-23160

Fig. 10.

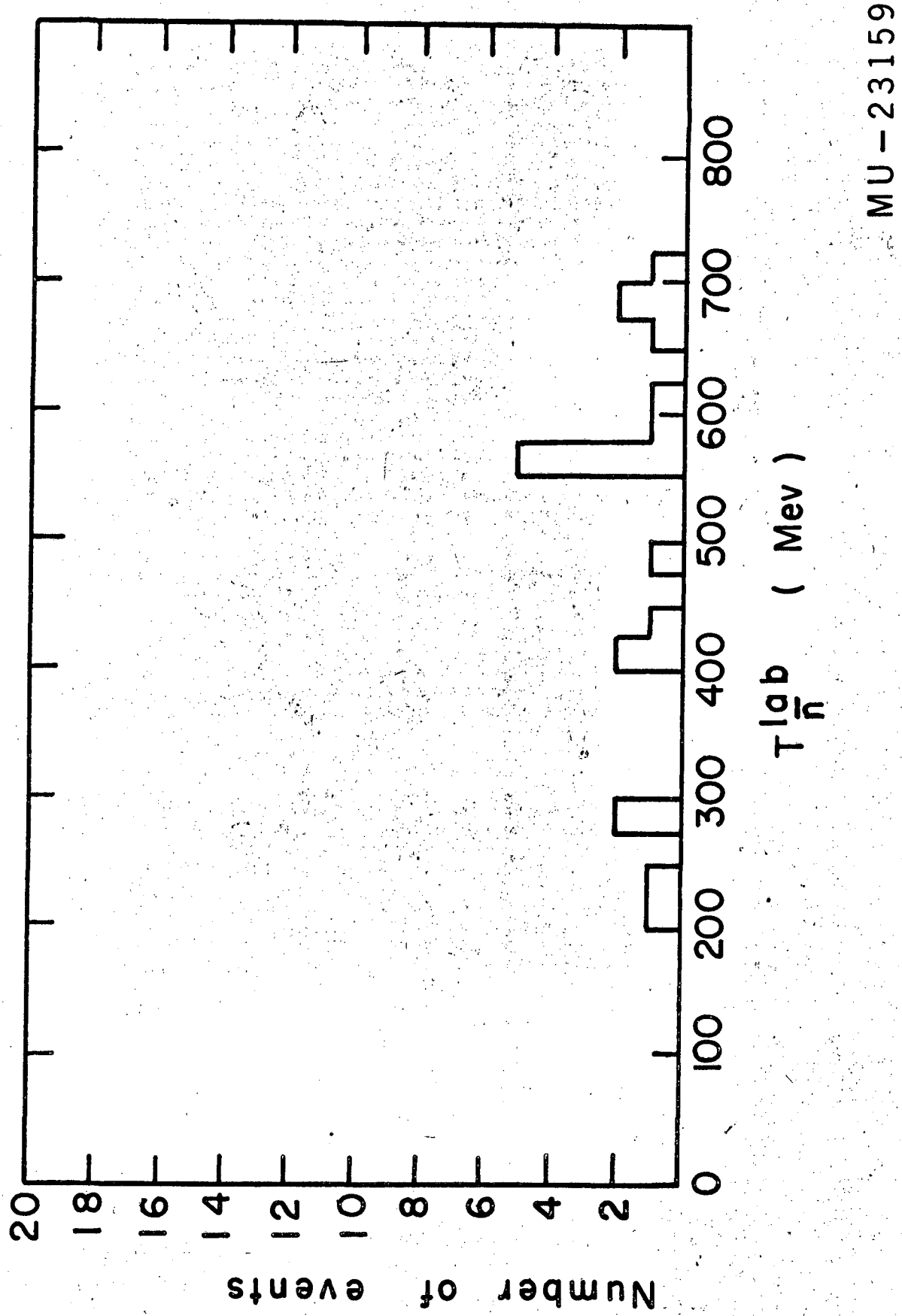
MU-23159
Number of events
0
2
4
6
8
10
12
14
16
18
20
100
200
300
400
500
600
700
800
T_n^{lab} (Mev)

Fig. 11

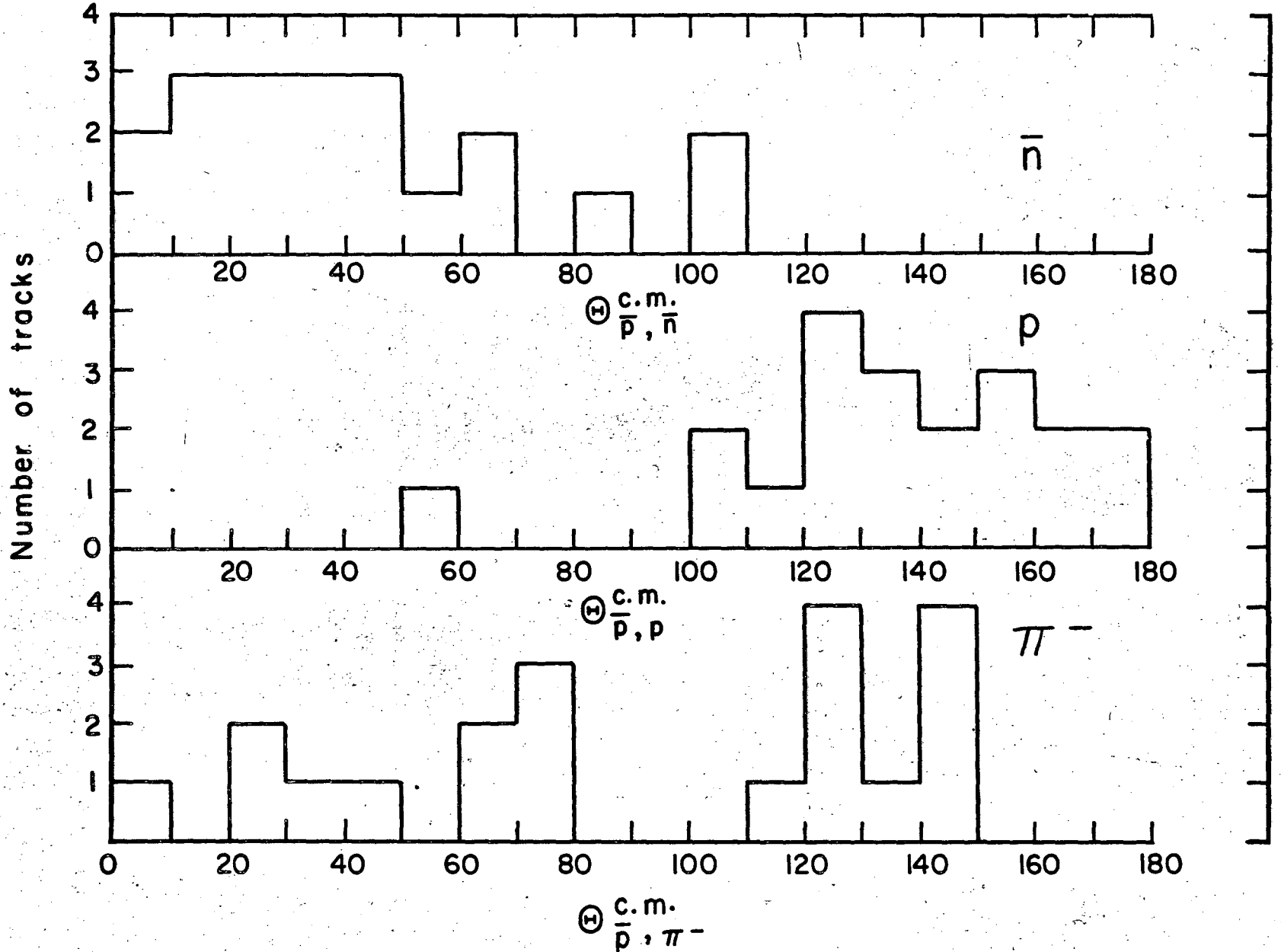

MU-23151

Fig. 12.

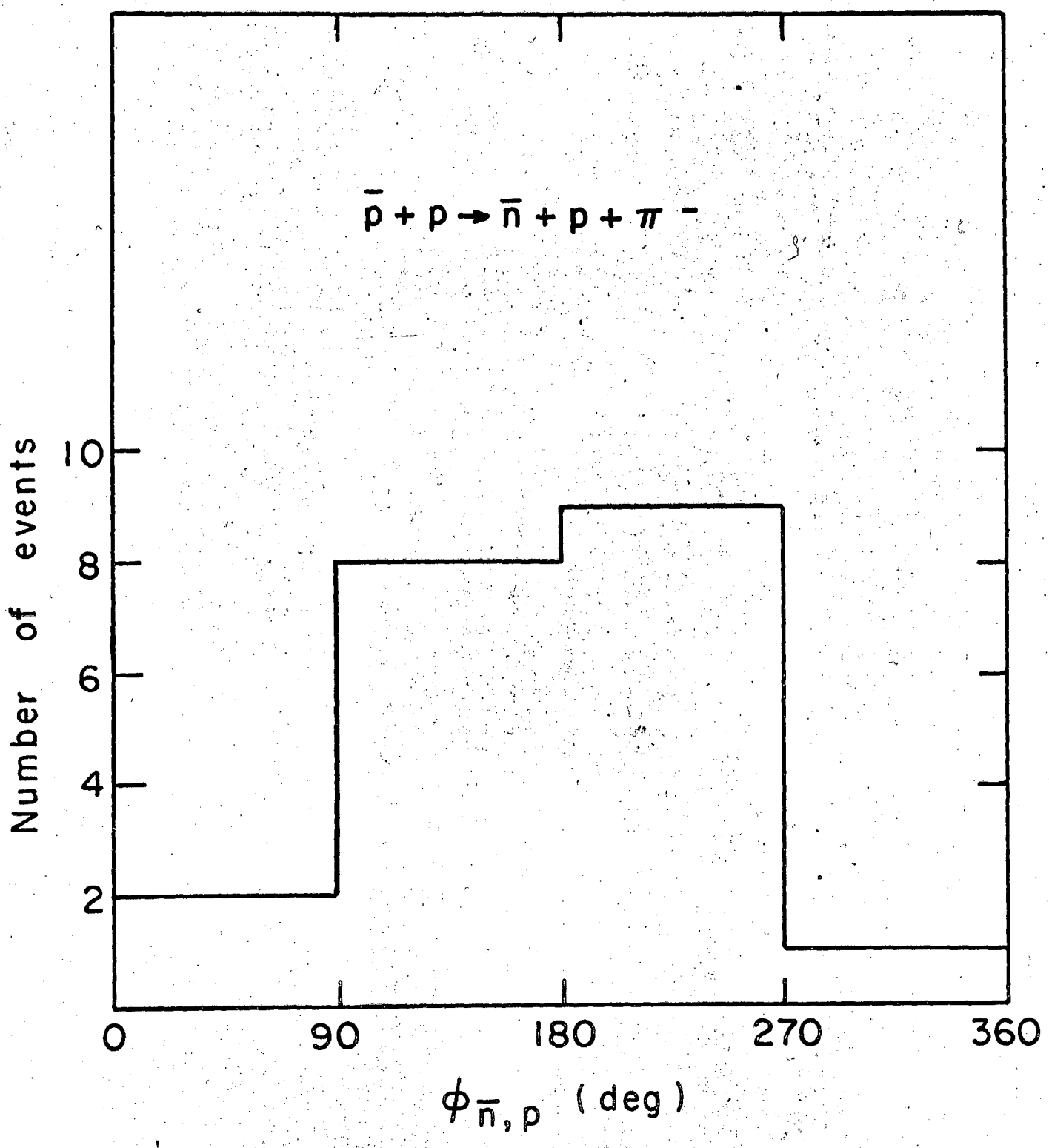
$\bar{p} + p \rightarrow \bar{n} + p + \pi^-$
Number of events
10
8
6
4
2
0
90
180
270
360
$\phi_{\bar{n},p}$ (deg)
MU-23157

Fig. 13

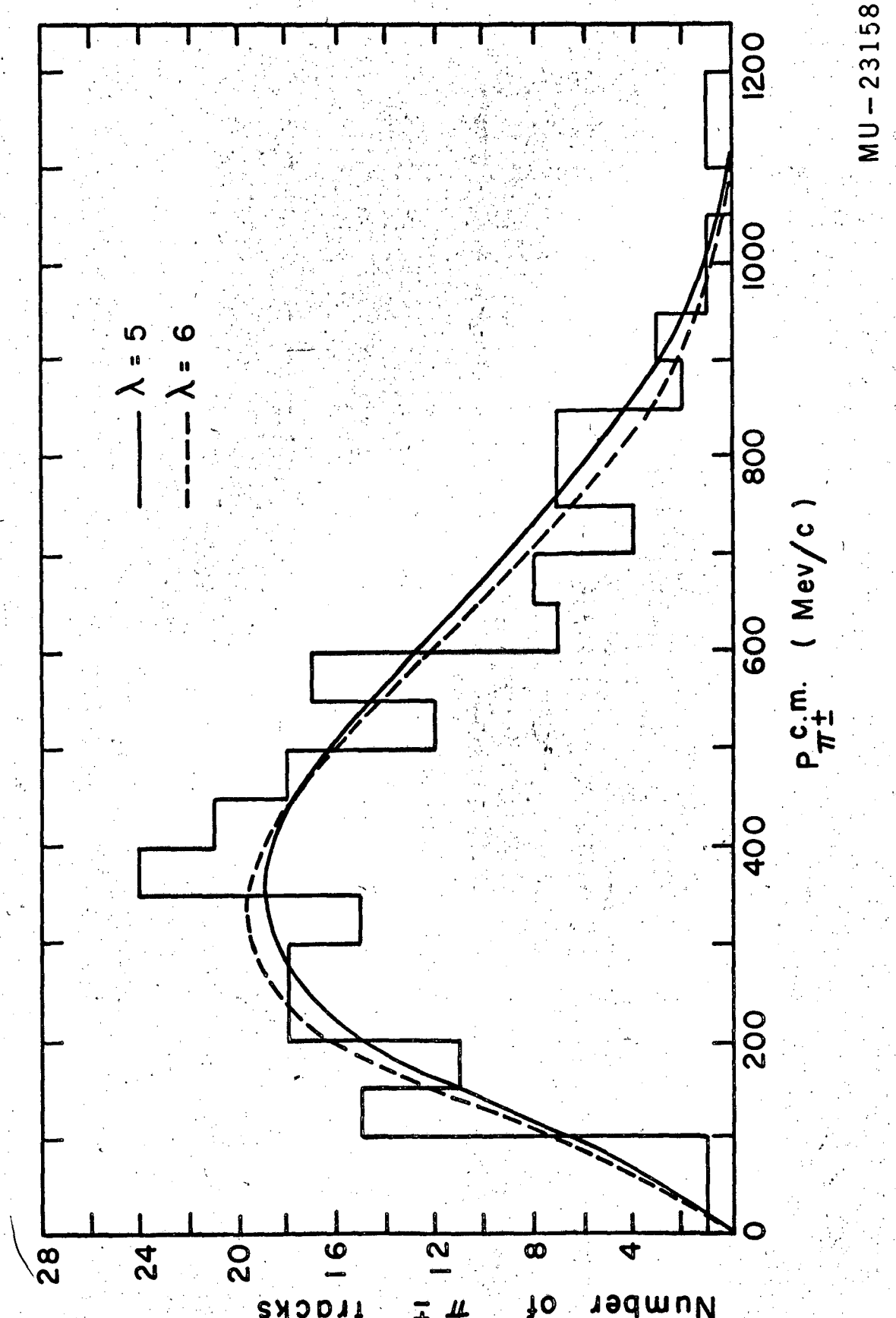
MU-23158
Number of π± tracks
$P_{\pi^{\pm}}^{c.m.}$ (Mev/c)
λ = 5
λ = 6
0
200
400
600
800
1000
1200
4
8
12
16
20
24
28

Fig. 14.

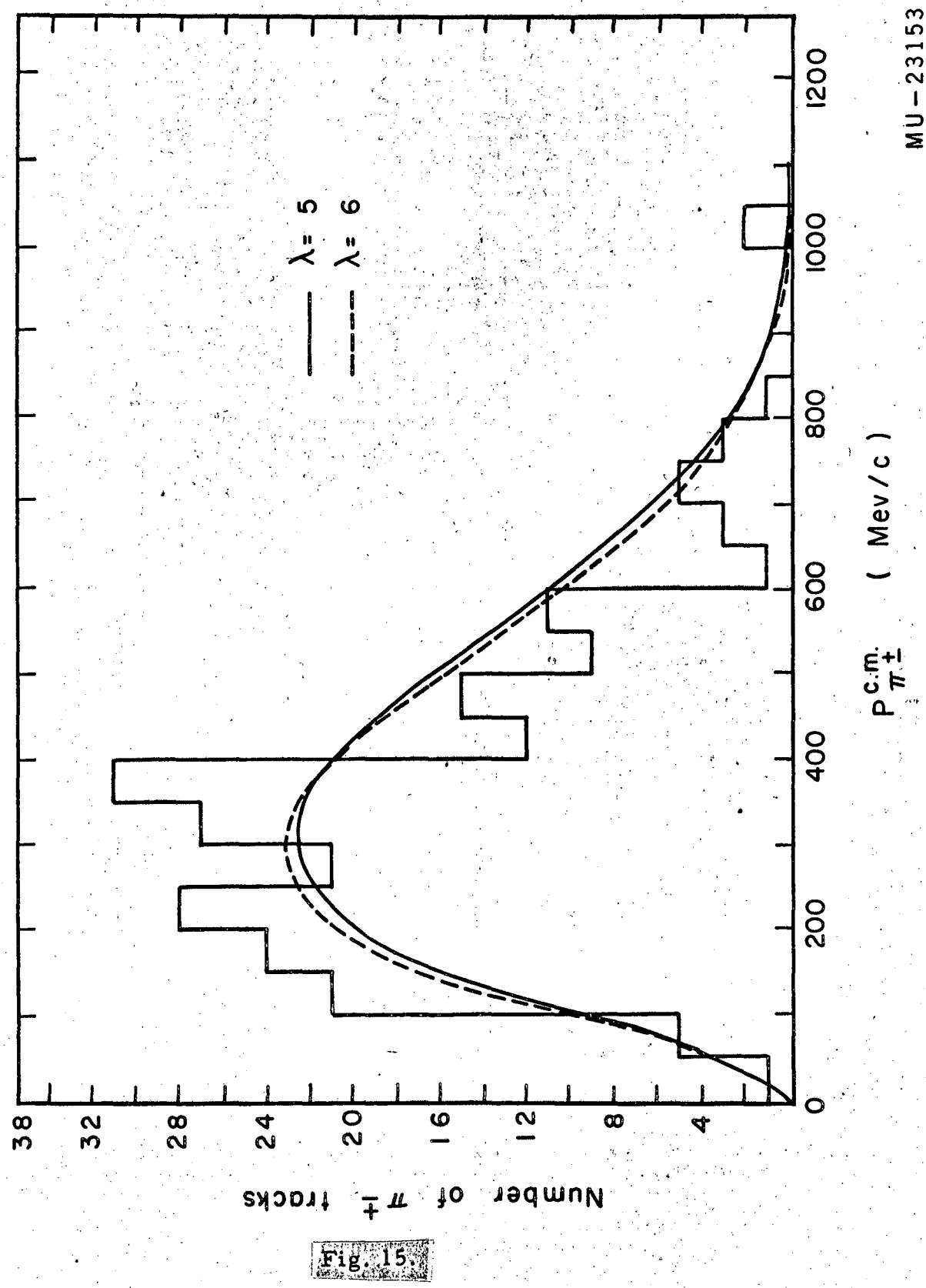
λ= 5
λ= 6
Number of $\pi^{\pm}$ tracks
0
4
8
12
16
20
24
28
32
38
200
400
600
800
1000
1200
$P^{c.m.}_{\pi^{\pm}}$ (Mev/c)
MU-23153

Fig. 15.

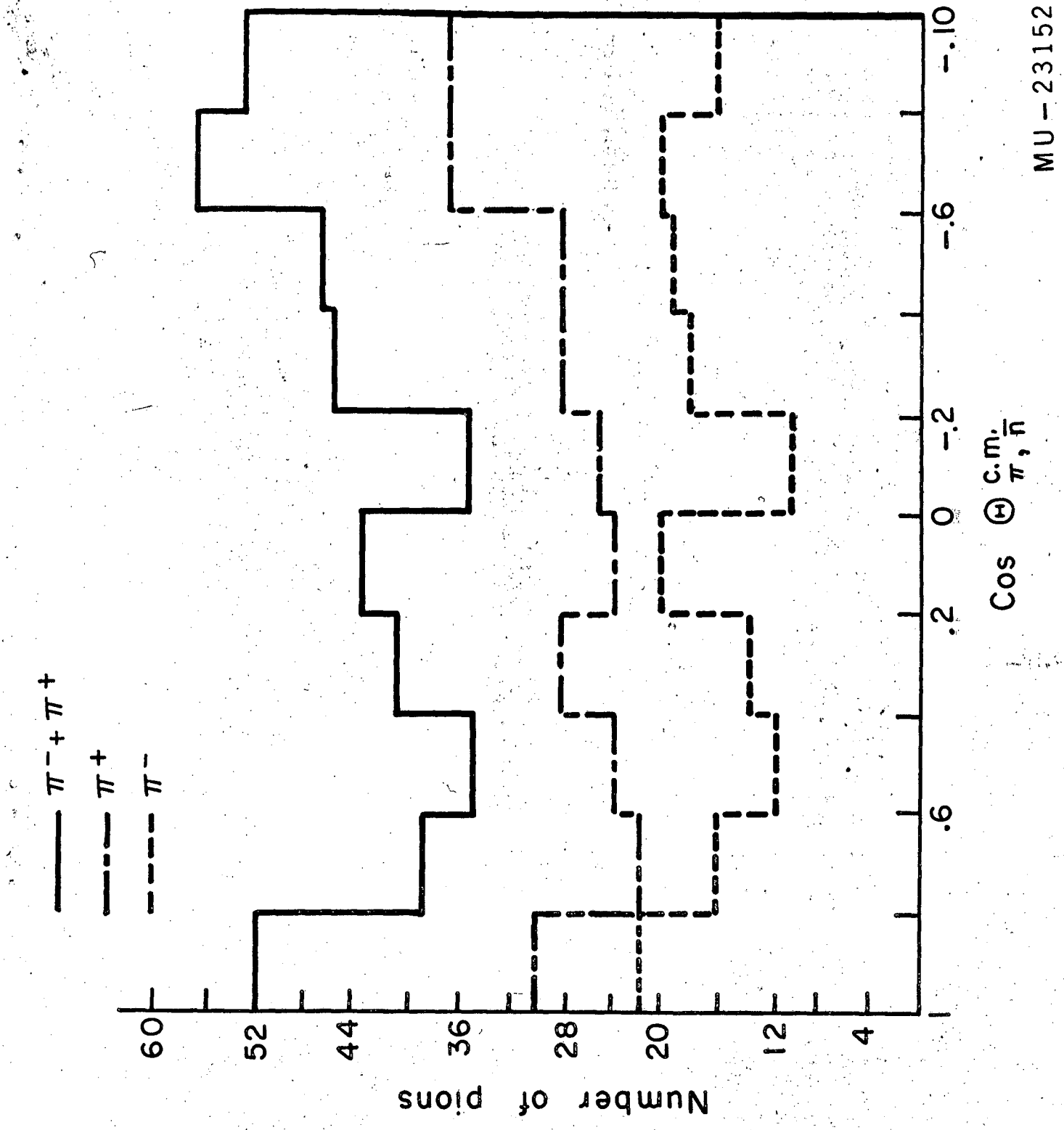
MU-23152
Number of pions
60
52
44
36
28
20
12
4
Cos Θ c.m. π, n
-.10
-.6
-.2
0
.2
.6
π⁻ + π⁺
π⁺
π⁻

Fig. 16